Polaris

Future Aircraft Design Concept

Team
Tobias Dietl
Jonas Karger
Katrin Kaupe
Andreas Pfemeter
Philipp Weber
Alexander Zakrzewski

Academic Support and Advisors
Institute of Aircraft Design, University of Stuttgart
Prof. Dr. Andreas Strohmayer
Ingmar Geiß

Contact: polarisaircraftdesign@gmail.com

Submitted on July 1st 2018

Universität Stuttgart

Universität Stuttgart
Institut für Flugzeugbau • Pfaffenwaldring 31 • 70569 Stuttgart

Institut für Flugzeugbau

Institutsleitung
Prof. Dr. Peter Middendorf
Prof. Dr. Po Wen Cheng
Prof. Dr. Andreas Strohmayer

Kontakt
Ingmar Geiß
Pfaffenwaldring 31
70569 Stuttgart
T 0711 685-60528
F 0711 685-62449
E-Mail:
geiss@ifb.uni-stuttgart.de
www.ifb.uni-stuttgart.de

Betreff: Bestätigungsschreiben

22.06.2018

Sehr geehrte Damen und Herren,

hiermit bestätige ich, dass die im Folgenden aufgeführten Mitglieder des studentischen Teams selbstständig den Flugzeugentwurf zur Teilnahme an der NASA/DLR-Design Challenge 2018 durchgeführt haben.

- Katrin Kaupe
- Tobias Dietl
- Jonas Karger
- Andreas Pfemeter
- Philipp Weber
- Alexander Zakrzewski

Mit freundlichen Grüßen,

Ingmar Geiß

Betreuender wissenschaftlicher Mitarbeiter

IFB
Institut für Flugzeugbau

Abstract

Looking at aviation in 2045 a competitive operation of aircraft will not only be dependent on highly efficient aircraft, but also on passenger comfort, manufacturing effort and an excellent life cycle.

The present report provides a breakdown of an aircraft design study with consideration of future aviation goals and proposals that might further improve the design with regard to pollutant and noise emissions.

An adjusted design process is used to find the synergies of all components and to combine their advantages instead of evaluating each component itself. Correlating with the design process, the final aircraft design is discussed with its results, options and challenges. To validate the quality of the results, the reference aircraft CSR-01 (A320) is emulated in relation to energy consumption, mass estimation and aerodynamics with a deviation of less than 1 %.

With special remark to the used key technologies the report provides information about current technical states, future improvements and an estimation of their qualitative efficiency in 2045. Except for high temperature superconducting (HTS) material all other used technologies are at least tested on a demonstrator or available for series production by now. HTS materials currently attain technology readiness level 4 and therefore illustrate that the used key technologies of this aircraft design are about to be available before 2025.

Finally, the improvements of this design are based on the synergistic integration of each component, resulting in a single-aisle transport aircraft that reduces the energy consumption for an equal mission by 61.39 % in reference to an A320 in 2005. A multi-functional fuselage concept combined with a calculated liquid hydrogen fuel system and a turboelectric power transmission complete the aircraft design reducing the energy consumption, manufacturing effort and increasing the reliability and passenger safety.

Contents

Nomenclature

Abbreviations

AC	Alternating current
BSCCO	bismuth strontium calcium copper oxide
CeRAS	Central Reference Aircraft data System
CFD	Computational Fluid Dynamics
CFRP	carbon fibre reinforced plastics
CG	Center of Gravity
CROR	Contra-rotating open rotor
DC	Direct current
FAR	Federal Aviation Regulations
GD	High- temperature superconductor
HPC	high pressure compressor
HTP	horizontal tail plane
HTS	High - Temperature superconductor
IATA	International Air Transport Association
ICAC	Initial Cruise Altitude Capability
IRA	Intercooled Recuperated Aero engine
ISA	International Standard Atmosphere
MAAMF	Mylar-aluminum/aluminum-Mylar foil
MAC	Mean aerodynamic chord
MTOM	Maximum Take-Off Mass
MME	Manufacturers Mass Empty
MZFM	Maximum Zero Fuel Mass
OPR	overall pressure ratio
OME	Operating Empty Mass
REVAP	Revolutionäre Arbeitsprozesse
SLI	single-line injection
SR	Short Range
TET	Turbine Entry Temperature
TLAR	Top Level Aircraft Requirements
TSFC	thrust specific fuel consumption
TOFL	Take-Off Field Length
UHB	ultra-high bypass
ULD	Unit Load Device
VARI	Vacuum Assisted Resin Injection
VeSCo	Ventilated Shear Core
VTP	vertical tail plane
YBCO	yttrium barium copper oxide

Symbols

Latin

Symbol	Description	Unit
L/D	glide ratio	–
c_D	drag coefficient	–
c_{Lmax}	maximum lift coefficient	–
$c_{L-Empennage}$	lift coefficient, empennage	–
$c_{Lmax,LDG}$	maximum lift coefficient, landing configuration	–
c_{Lmax}	maximum lift coefficient	–
$\dot{m}$	decision speed	kg/s
v_1	mass flow	m/s
$v_{s,TO}$	stall speed, take-off configuration	kts
$v_{s,LDG}$	stall speed, landing configuration	kts
$V_{VTP,MTOW}$	Volume coefficient for the vertical tail in MTOW configuration	–
$V_{VTP,OEW}$	Volume coefficient for the vertical tail in OEW configuration	–

Greek

Symbol	Description	Unit
α	angle of attack	rad
$\alpha_{empennage}$	angle of attack, empennage	rad
$\gamma_{approach}$	approach angle	deg
η_{th}	thermal efficiency	–
$\eta_{th,baseline}$	thermal efficiency baseline	–

List of Figures

List of Tables

1 Introduction

A look back at the last years shows that the number of flight movements rose each year to approximately 42 million in 2017 [1]. This number will rise further due to lower fares and increasing flight routes for the foreseeable future. As a matter of fact, it is necessary to consider new aircraft configurations and propulsion systems as well as the synergistic integration in the complete aircraft to reduce the energy consumption of transport aircrafts drastically. Beyond that innovative operating concepts and air operations need to be considered as well [2].

This report focuses on the design of a new single-aisle transport aircraft, using an A320 as reference. The Best-in-Class version of the A320 from the year 2005 is specified with a design range of 2750 NM at a design payload of 13 608 kg. An own investigation of the A320s' actual flight range shows that the largest number of flights is below 1500 NM [3]. In the future new flight routes might be necessary to match customer expectations, but it is a matter of fact that a mission sector of 1500 NM covers nearly all destinations in Europe, Asia and North America. The investigation therefore considers 1100 flights on 19 airports in these continents, as these flights will still be part of future aviation. Figure 1.1 shows the number of flights for its flight distance and the percentage of flights in total. A range of 1500 NM covers 85 % of the investigated flight and as there are only a few flights above 2200 NM, the chosen design point of the present concept is set to 1500 NM at a payload of 13 608 kg.

For the validation of the present design concept, the A320 is emulated for this design mission. The RWTH Aachen provides a Central Reference Aircraft data System (CeRAS) [4], in this the CSR-01, a modeled A320, is used. It fulfills the requirements of the task and provides all necessary data from a single source. The advantage of using the CSR-01 A320 model lies in having validated information about an A320 regarding the propulsion system, aerodynamics, mass breakdown and performance. The final design concept is compared to the model with the exception of a changed design point. Table 1.1 shows the Top Level Aircraft Requirements that are chosen for the design.
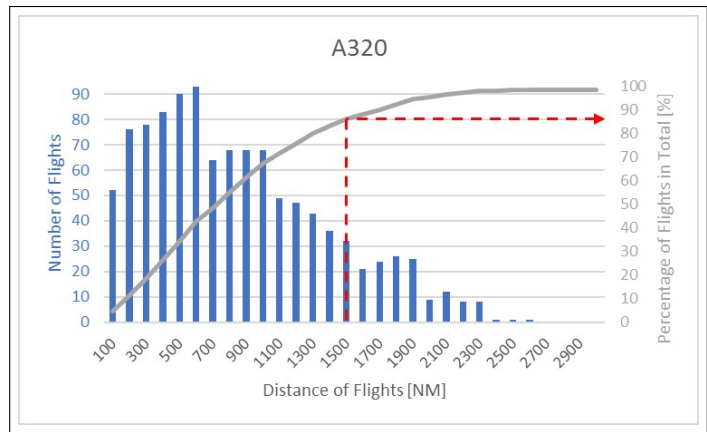
Figure 1.1: *Operation evaluation of the A320*

Table 1.1: *Top Level Aircraft Requirements*

		CSR-01	*Polaris*			CSR-01	*Polaris*
Mission Range	[NM]	2750	1500	ICAC	[ft]	33000	33000
Alternative	[NM]	200	200	TOFL	[m]	2200	2200
Payload	[kg]	13608	13608	Approach Speed	[KCAS]	138	138
Passengers	[-]	150	150	Wing Span Limit	[m]	36	36
Cruise Mach	[-]	0,78	0,72	Turnaround	[min]	30	30

2 Design Decisions

"Every revolution in aviation technology came
from modification of the propulsion system, [..] the next leap may very well be electrical propulsion in which
superconductivity would be the enabling technology."

- P.J. Masson et al in *Superconductor Science and Technology*, June 2007

Polaris combines the efficiency of a superconducting electric propulsion system with an improved gas turbine cycle in a turboelectric propulsion chain, while using cryogenic liquid hydrogen not only as fuel, but also to cool between compressor stages and simultaneously enable superconductivity at the electric motors and generators. Consequentially, a high level of synergy and efficiency can be achieved with the system as a whole. A contra-rotating open rotor transfers the power with minimal losses onto the air, ensuring increased efficiency from fuel all the way to the air. This propulsion system is complemented by a multi-functional fuselage concept, which is designed to carry the fuel volume while at the same time reducing the fuselage weight by 28.7 % and increasing the fire and crash worthiness. Part of the multi-functional fuselage is the gondola concept. In difference to the A320 fuselage, the fuselage is separated in a primary and a secondary structure. While the primary structure is still carrying the pressure cabin and necessary systems, the secondary structure is an unpressurized housing for the LH_2 fuel tanks (see figure 2.4).
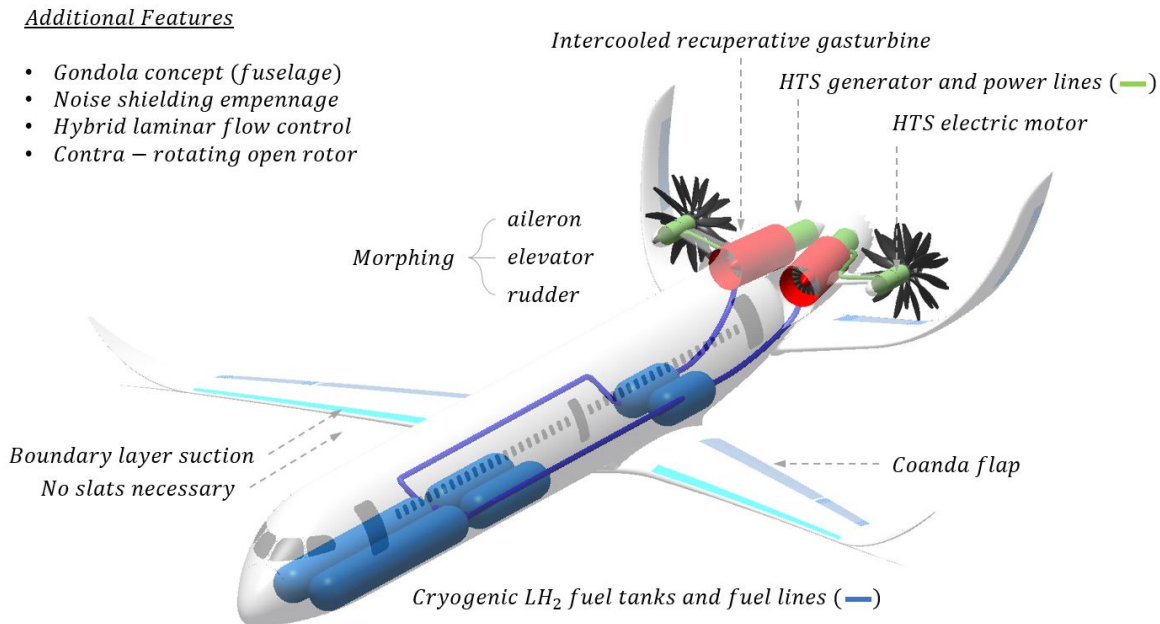
Figure 2.1: *Polaris*

Using a systematic evaluation process, various propulsion architectures and aircraft configurations have been assessed qualitatively regarding their capability to combine synergies. The design features are part of the design process with the goal to reduce the energy consumption for the design mission. *Polaris* is the result of this design process with respect to fulfill future aviation tasks.

2.1 Design Considerations

Level 1

The first level shown in figure 2.2 focuses on the propulsion unit. Two promising concepts are the Ultra-High-Bypass fans (UHB) and the Contra-Rotating Open Rotor concept (CROR). According to a study made by the NASA in 2013, the predicted propulsion efficiency of the CROR is with $> 90\,\%$ above the efficiency predicted for UHB fans [5]. This is however with a restriction to the cruise speed, as the propulsion efficiency rapidly drops above a certain Mach-number. As the focus lays on overall efficiency the CROR is given preference. In a first estimation the gain in efficiency is assumed worth the mission time trade-off. This trade-off is reevaluated at a later stage, as described in section 6.2.

Level 2

Level two contains two different kinds of power transmission. While a geared fan needs the turbine, shaft and propeller to be outside of the fuselage as a whole, the electric transmission is designed with turbine and generator inside the fuselage and an electric motor with its propeller outside. Due to a smaller diameter of an electric motor compared to the turbine, the electric driven structure has the advantage of an increased propeller integration efficiency, as

Figure 2.2: *Design Process*

the propeller wash is subjected to less wetted area. The electric transmission enables cross-wiring from the generator to each electric motor and by that allows all electric motors to operate even in case of a turbine or generator failure, cf. section 3.1.

Level 3

A highly discussed topic for future aircraft designs are different hybrid systems, e.g. as shown in figure 2.3. In general the three architectures "battery-assisted", "fuel-cell-assisted" and "turbo-electric" comprise the most common systems. To select the correct hybrid system it is unavoidable to take care of the provided power and the needed energy. While all three hybrid systems improve comparable current propulsion systems, only the turbo-electric system is able to provide the power needed for single-aisle transport aircrafts with regards to the overall mission energy consumption.

Using batteries the division between high-energy and high-power batteries has to be taken. Every battery has either a high energy density or a high power density. To power an aircraft with maximum take-off mass (MTOM) above 50 tons at least 20 MW are needed. A current calculation of a battery system for passenger aircrafts gives a power density of 0.822kW/kg [6]. A purely electric flight for a single aisle, 150 passenger aircraft would not be feasible. Because there are no sufficiently accurate sources for future specific power densities of batteries, an estimate has been made. As high-power batteries might enable 3 kW/kg in 2030, a total battery weight of more than 6.6 tons will be necessary (at an energy density of 0.24 kWh/kg). The additional battery mass rises the total mass of the aircraft and requires a higher power performance. High-energy batteries might reach 0.6 kW/kg which causes a ten times higher battery mass for the same power output. For the design process calculations are made to validate a support of the batteries to the required power. In regard of the complete system, neither high-energy batteries, nor high-power batteries will match an improved propulsion system and therefore lead to a higher energy consumption for the mission in any case.

Fuel-cells are facing the same challenge with energy and power densities, which depend on the size of the cells and enlarge the fuel-cell system by such an amount, that they are ineffective for this aircraft category. Going to a seat number below 70 such hybrid systems gain more importance and might revolutionize commuter aircrafts.
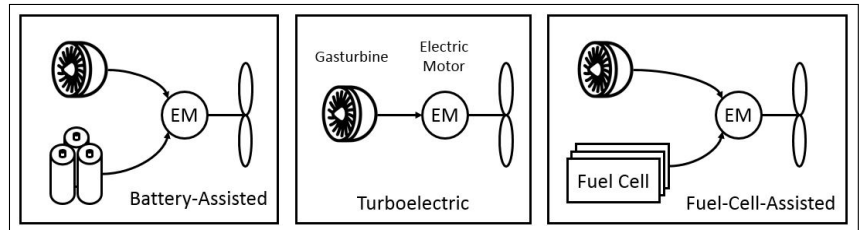
Figure 2.3: *Different Hybrid Systems*

Level 4

Another significant change is made by using new fuel types. Although kerosene can be produced synthetically, these biofules still have comparable pollutant emissions to kerosene and therefore will not meet future aviation emission goals. Using hydrogen, an energy densities of 33 kWh/kg is usable what is nearly three times as much as the energy density of kerosene (12 kWh/kg) or methane (14 kWh/kg).

The challenge of using hydrogen is its gaseous state at ambient temperature. Gaseous hydrogen has a density of $0.09\,kg/m^3$, while kerosene has a density of $800\,kg/m^3$. This causes the volume of hydrogen at 273 K to be nearly 9000 times bigger than kerosene. To solve this challenge it is either possible to store the gas at up to 700 bar or to store it liquid at 20 K, which is also called cryogenic. In order to use synergies it is an advantage to use the liquid hydrogen (LH_2) to cool the gas turbines, generators and electric motors. The combustion of hydrogen in a gas turbine prevents all of the pollutant emissions with exception of NO_x and H_2O, which is discussed in section 6.1.

Level 5

While the blended-wing-body offers advantages at a number of passenger above 600 it is inadvisable to take this concept for a single-aisle transport aircraft due to its large wing area and lift, because of which the optimum L/D can't be met during cruise [7].

The challenge of carrying enough liquid hydrogen for the operation of a single-aisle transport aircraft is to provide sufficient space inside the fuselage or wing. The large fuel tanks cannot be integrated in the wings due to their geometry. However the gondola concept enables the integration of the fuel tanks inside the fuselage, but outside of the pressure cabin. With the combined advantages of each level the required volume of LH_2 is reduced to a minimum, allowing the LH_2 to be stored completely inside the gondola without using space for e.g. landing gear, wing box or electrical systems, while furthermore achieving the smallest fuselage area. This is described in detail in section 3.2.

With equal dimensions to the reference aircraft, *Polaris* does not force the airport infrastructure to change significantly. It is not a boundary condition for these design decisions to avoid infrastructural or airspace modification, however it is shown that such modifications are not necessary by using synergies of each level for single-aisle transport aircrafts.
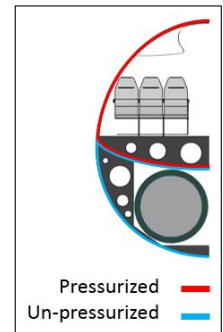
Figure 2.4: *Different Hybrid Systems*

3 Key Technologies

Achieving radical energy and emission reductions require highly efficient and unconventional propulsion and structural desigs. In the following chapter the used propulsion architecture and structural advancements are presented, key technologies discussed and their synergies outlined. Every key technology is picked upon its potential of improvement over state of the art technology and their respective viability.

3.1 Propulsion Chain
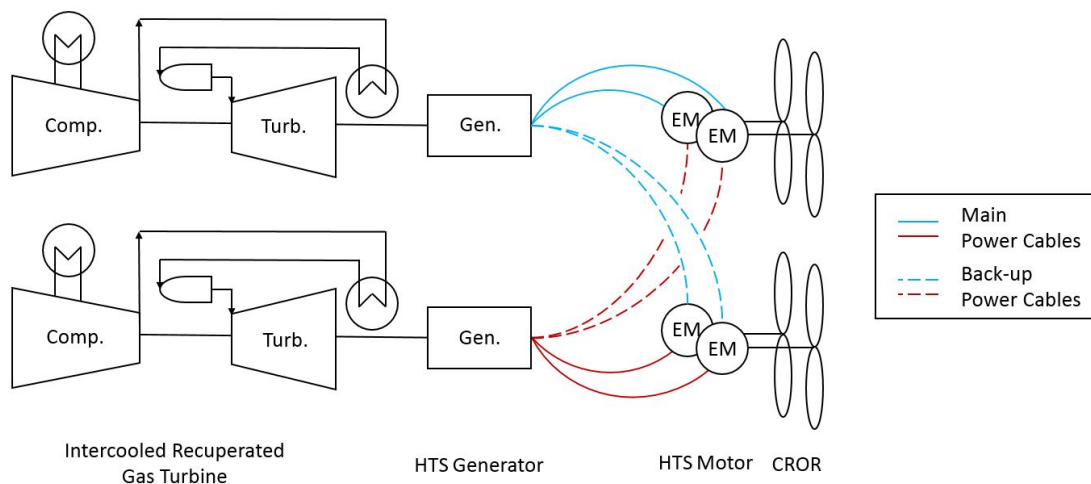
Figure 3.1: *Turboelectric propulsion chain of the Polaris concept*

The concept of a turboelectric propulsion system consists of a gas turbine, generator and electric motor driving two contra-rotating propellers. The two CRORs are used as propulsors, whereas the gas turbine is solely used to produce shaft power. The power generated by the turboshaft is transformed into electric energy through a high temperature superconducting (HTS) generator.

The coupling between generator and electric motor acts as electric transmission, which allows both the gas turbine and the CRORs to run at their respective optimum speeds. Electrical cross-wiring between the generators and the electric motors, as seen in figure 3.1, enables all electric motors to continue to operate in case of a generator or gas turbine failure. To maintain the same speed ratio of electric motors and gas turbine,

the variable-pitch propeller decreases the power loading at the same speed to match the reduced power provided by the remaining gas turbine.

Gas Turbine

Present gas turbine cycles reach their limits when it comes to an improvement of energy efficiency or thrust specific fuel consumption (TSFC) along with a reduction of NO_x emission. Designing a gas turbine at high load levels for best core efficiencies causes high cycle temperatures. Parametric optimization of a two-spool turboshaft in GasTurb 13 shows, that high cycle temperatures require high overall pressure ratios (OPR) to attain best core efficiencies. An optimization of TSFC therefore pushes the formation of NO_x, as formation mechanisms show an exponential dependency on cycle temperatures [8].

New gas turbine concepts are currently under investigation by numerous research centres and industrial partners. Regarding the 2045 time frame of *Polaris*, the intercooled recuperative aero engine (IRA) concept shows the most promising cycle technology [9]. Intercooling reduces the specific power demand of the high pressure compressor (HPC), as the mass flow is cooled down between compressor stages. The work needed by the HPC to enhance OPR is decreased as the temperature at its entry is falling [10]. Recuperation benefits from increasing spread in temperature between exhaust mass flow and compressor mass flow, thus enabling higher temperature levels in the combustion chamber without manipulating fuel flow [10]. IRA cycles show the ability of higher core efficiencies for an OPR of up to 40, see figure 3.2.

As part of the project "Revolutionäre Arbeitsprozesse" (RE-VAP), multiple IRA cycles have been investigated using the key technologies intercooling, recuperation, isochoric combustion with a wave rotor or pulse detonation and sequential combustion [12]. They concluded, that intercooling and recuperation enables the thermal efficiency to increase by 7 %-13 % to the baseline of $\eta_{th,baseline} = 42\,\%$ [12] for an overall engine. Although isochoric combustion may lead to even higher thermal efficiencies, this technology is neglected in the design process as there is insufficient performance simulation and poor knowledge about its negative impact on turbine behaviour due to unsteady exit conditions [13]. Contrary to the estimated values of the bare IRA cycle, presented in figure 3.2, these thermal efficiencies are calculated using a tailored engine model. This model is taking losses due to propulsor, component cooling and minimum tip height into account. For a more realistic assessment of gas turbine efficiencies, the following calculations will consider the values as concluded by REVAP.. As part of the program, an optimization of the IRA cycle performed by TU

Figure 3.2: *Core efficiency of different engine concepts [11]. For OPR up to 40, efficiencies of IRA cycles are exceeding compared to Joule cycles.*

Dresden proved thermal efficiencies of $\eta_{th} = 50.8\,\%$ for a moderate OPR of 40 and 1590 K TET. Reaching equal thermal efficiencies for a conventional Joule cycle, requires an OPR of 99 and 2000 K TET [14]. New combustion technology and the reduction of OPR and TET are main drivers for low NO_x combustion [8].

Employing IRA into the *Polaris* concept yields some additional advantages regarding intercooler technology. Using LH_2 as coolant exhibits high efficiencies of the intercooler, allowing its surfaces to be minimised. Intercooling during critical operating conditions, such as take-off and climb, remains possible with a LH_2 cooling architecture, where otherwise the cooling air mass flow for conventional bypass architectures might not be sufficiently provided.

More synergies are found regarding the reduction of bleed air temperature, therefore optimizing the cooling of hot components and simultaneously enabling a reduction of bleed air mass flow which raises core efficiency [10].

Superconducting Technology

Cycle studies during the REVAP program proved the necessity of a separation of propulsor and power generation if engine architecture shall be optimized - which is therefore realized in the *Polaris* concept. As described above, decoupling the rotational speeds of gas turbine and propellers allows them to run in their respective optimum, as generator and electric motor are acting as "electrical gearbox" [15]. Furthermore, a turboelectric architecture enables an independent positioning of propulsion chain components.

Incorporating conventional systems in turboelectric propulsion chain architecture is not practical for the *Polaris* concept, as power densities of electric motors and generators are too low; but superconducting technology becomes a key enabler for these systems [16], see figure 3.3. Moreover, using liquid hydrogen both as propellant
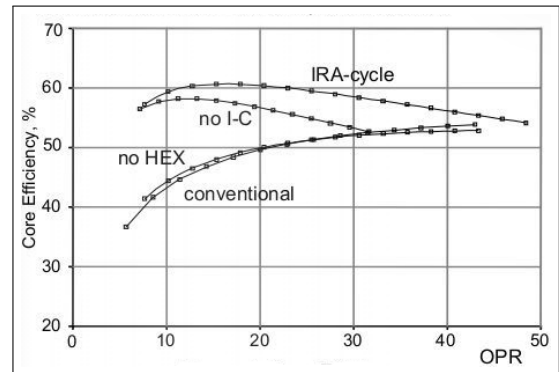
and coolant for superconducting wires, cooling is practically free because liquid hydrogen must be evaporated before being burnt.

HTS technology, discovered in 1986, exhibits high current densities at very low resistance. Fully superconducting machine designs , using HTS winding both on rotor and stator, show power densities up to 40 kW/kg at rotational speeds of about 10,000 rpm [17].

Several institutions have already realized partially superconducting systems, thereunder General Electric's Homopolar Inductor Alternator with a power density of 8 kW/kg [18]. Partially superconducting machines use superconducting windings on the rotor where DC currents induce a DC magnetic field, interacting with copper stator windings which are excited with alternating current. Current superconducting material like BSCCO and YBCO shows AC losses which make their use as stator windings impractical until now [16]. A lot of effort on research for low AC loss HTS material is done by several research centres and companies. According to the American Institute of Physics, MgB_2 with a critical temperature of 39 K and best performance under 30 K, shows high potential to reduce AC

Figure 3.3: *Power densities of superconducting and conventional electric machines [17]*

losses when arranged as fine, twisted filaments [16]. Liquid hydrogen is on a temperature level well below the critical temperature of MgB_2 thus improving its current carrying capacity [19].

Based on NASA's technology roadmap, power densities of HTS machines - including generators and motors - are predicted to be as high as 33 kW/kg [20]. Further calculations for the *Polaris* concept will use a more conservative value of 20 kW/kg.
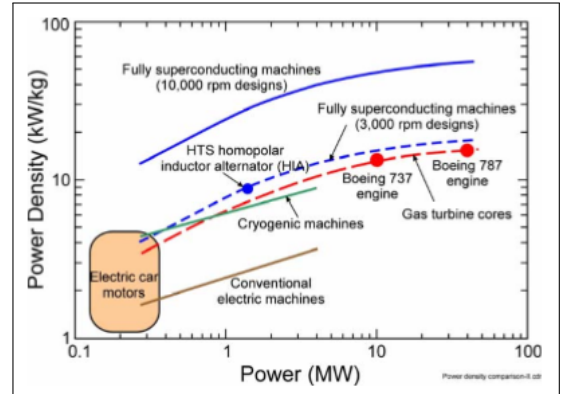
Contra Rotating Open Rotor

Increasing efficiencies of the propulsor inhibits potential for further optimization of the propulsion chain. Studies by NASA, General Electrics and the Federal Aviation Administration have stated propulsive efficiencies of 96 % [5] for open rotor concepts compared to 65 % [21] for conventional fans. In addition, an advantage of open rotors is their compact integration.

The open rotor concept uses two contra rotating propellers in pusher configuration mounted on two hollow shafts. Assembling two propellers in one line removes the rotational flow produced by conventional propellers, former present losses are transformed in additional thrust which enables higher propulsive efficiency. As previously stated, high power densities for superconducting electric motors allows them to be small, thus reducing friction drag and simultaneously downsizing the shadowing effect on the propellers mounted on the aft of the electric motors. Reduced shadowing of the propeller in turn decreases blade loading and therefore achieving an overall efficiency of 95% for the electric components of the propulsion chain. Further investigations on CROR technology is active, Safran previously validated present assumptions by running a successful test on a compact rotor concept demonstrator.

Major concerns and misinterpretations on the open rotor concept pertain to the assumption of increased noise levels. However, studies as from NASA [22] and field tests conducted by Safran have proved a reduction of noise emissions compared to enclosed engines. Moreover, CFD analysis [22] has shown, that noise emissions of pusher configurations are more uniform compared to tractor configurations. In order to further reduce the noise emissions during flight, the propellers are shielded by the H-Tail in downward direction.

Flight Mach number has to be reduced from $Ma = 0.78$ to $Ma = 0.72$ due to efficiency losses and noise issues which go along wing tip speed. However, this does not infringe current flight missions, as time losses per flight leg are minimal. A detailed analysis of the mission is shown in chapter 5.

3.2 Multi-functional fuselage concept

A further reduction of the energy consumption can be achieved by minimizing the structural weight of the aircraft with a multi-functional aircraft structure. With carbon fiber reinforced plastics (CFRP) an advanced technology is applied to reduce the structural weight and the manufacturing effort. The special feature of the Gondola Concept is the further partition of a primary and a secondary fuselage structure. *Polaris* uses this concept to minimize the structural weight and to integrate the fuel tanks outside of the pressure cabin. The present design is developed regarding weight, passenger safety, crash worthiness and manufacturing advancements.

According to the final report from the German Aerospace Center (DLR) a fuselage weight reduction of 28.7 % is achieved. Thishas been validated with a demonstrator using tests that fulfill current certification criteria [23].

Integral Shell Design

At present, structural elements are manufactured as monolithic CFRP by using a skin, stringers and frames (e.g. A350, B787). As the bonding of these elements is not certified today, the usage of rivets is necessary to achieve a certified joint. Therefore, the fuselage is manufactured with CFRP with less reduction of the structural weight, as rivets weaken the CFRP and require higher material thicknesses.

A significant advancement to current CFRP fuselages is the use of a load-bearing skin. The sandwich structure consists of a detector layer, an inner layer and a support material between these layers. Furthermore, individual layers are combined with the outer layer to fulfill crash and fire resistance requirements [23]. The DLR analysed and tested a demonstrator regarding:

- impact and residual strength behaviour,
- 3D-thermal-analysis,
- 3D-tension and stress analysis,
- stability against buckling,
- fire safety,
- crash safety,
- high velocity impact,
- manufacturing effort and costs.

The integral shell design is developed to withstand crash and impact. Using phenolic resin, a fire resistance is achieved to block toxic vapors, smoke and a burn-through for minimum 15 minutes at 1100°C.

The foam core has a secondary function as crash absorber and separates the detector layer and the inner layer. In case of an impact, the detector layer is damaged and delaminated close to the impact. A maintenance of the inner layer is not necessary, as such the time necessary for repair is reduced. Replacing the foam core with a Ventilated Shear Core (VeSCo) reduces the weight of the Integral Shell Design furthermore, drastically reduces the number of parts (less frames, no stringers) and allows a long-term stability due to a ventable foldcore sandwich [24]. Different to foams, humidity is not kept inside the foldcore while the structure is ventable with air.
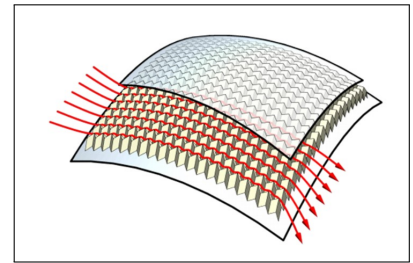

Figure 3.4: *VeSCo Concept [24]*

Gondola Concept

Similar to the A320 fuselage the primary structure of the Gondola Concept includes the pressure cabin to carry passengers and the crew. As it is not necessary to change the cabin arrangement, the passenger area of the A320 is taken as template. Unlike the A320 fuselage this pressure cabin does not include the cargo area of the aircraft. With CFRP a pressure cabin is designed without the need of a fully circular shape. The advantage is a primary structure that carries only the most necessary contents which require a pressurized environment. Regarding a malfunction of the fuel tanks, any security incident with respect to fire, smoke or toxic vapors must take place outside of the passenger area (figures 2.4 and 3.5). To guarantee this requirement a placement of the fuel tanks outside of the primary fuselage structure is realized. LH_2 fuel tanks, landing gear, wing, empennage and propulsion system are attached to the primary structure (figure 4.2).

The secondary fuselage structure is designed as a non-load bearing and unpressurized area that houses the fuel tanks and cargo. Furthermore, the secondary structure is developed as a "sacrificial structure" regarding crash/impact. While this area is not pressurized there are less demands on the structural strength and cargo doors need not to be as sealed as one in the pressure cabin. A malfunction of the fuel tanks does not affect the passenger area, as fire, smoke and toxic vapors cannot get into the pressure cabin.

Manufacturing

With current technologies to manufacture CFRP structures using liquid resin infusion technologies (SLI, VARI, etc.), the size of shell parts is limited by the autoclave length ($< 25m$). At present it is possible to fit the primary structure together out of 2 longitudinal and 3 transversal joints. The future manufacturing time and effort can be drastically reduced by producing larger subcomponents and a CFRP structure with a minimal number of rivets can be certified [23]. As per statement of the DLR a cost reduction of -40 % can be achieved.

Figure 3.5: *Gondola Concept*

Another significant advantage is the quality assurance, as less joints are necessary and the autoclave process can be controlled and logged. Overall the primary energy consumption is reduced due to decreasing waste amounts, an optimized manufacturing process and innovative mounting technologies [23].
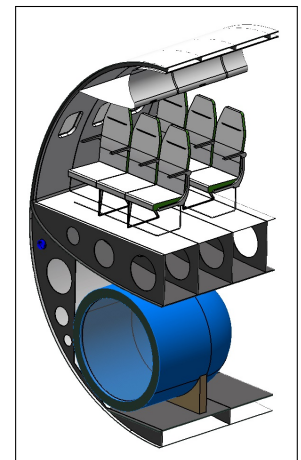
3.3 Aerodynamics

Polaris' advanced aerodynamic layout allows an improvement of the glide ratio during cruise by 18 % to L/D=20.23. This improvement is mainly a result of a minimization of turbulators on wings and fuselage while focusing on long laminar airflows, which are achieved by passive and active means. For this purpose the forward swept wing and the morphing wing technology and a special surface finish [25], as well as a boundary layer control system and the coanda flaps are installed.

The calculation of lift-dependent drag is performed in XFLR5 [26] and OpenVSP, whereas non-lift-dependent drag is estimated using handbook methods. Using these methods CeRAS' aircraft polar could be reproduced and used to calibrate further calculations.

Adressing the non-lift-dependent drag a special surface finish, creating a riblet structure [25] can be used. This creates a similar turbulator effect as in golf balls, reducing the drag of all components in turbulent airflow by up to 8%. The full drag estimation for non-lift-dependent components can be found in figure 3.1.

Table 3.1: *Non-lift-dependent component drag*

Fuselage	0.2450
Winglets	-0.0022
Cockpit	0.0850
Gas Turbine & Inlet	0.0574
Engine Struts	3.5E-05
Engine Pods	0.0511
Interference Drag	0.0063
Total (referenced on the wing area)	0.0130
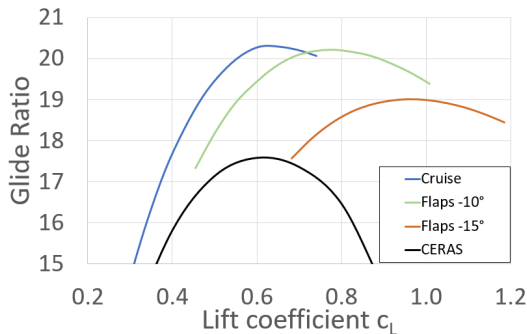
Figure 3.6: *L/D Polars of Polaris and the reference aircraft CeRAS*
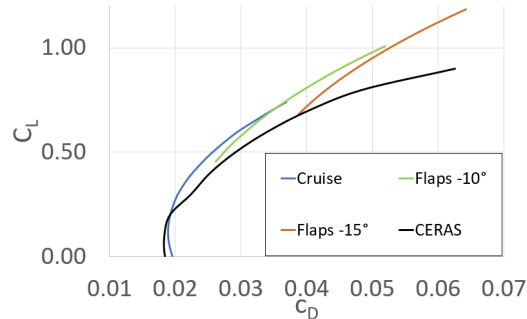
Figure 3.7: *$c_L - c_D$ polars of Polaris and the reference aircraft CeRAS*

Forward Swept Wing

Usage of a forward swept wing configuration allows to reduce the wing's aerodynamic sweep angle compared to a conventional backward swept wing while maintaining the same geometric sweep angle [27]. The higher the aerodynamic sweep angle, the stronger the disturbances on laminar flow influencing laminar-turbulent transition as cross-flow instabilities and attachment line transition. Although a reduction of both sweep angles can be similarly achieved with a conventional backward swept wing configuration, a high geometric sweep is desired to delay shock waves on the wing [28]. The optimal sweep angle for *Polaris* is derived from Krause [29] and Hepperle [30] as an exact estimation and optimization of the sweep angle are out of scope of this report and have to be analyzed separately. In combination
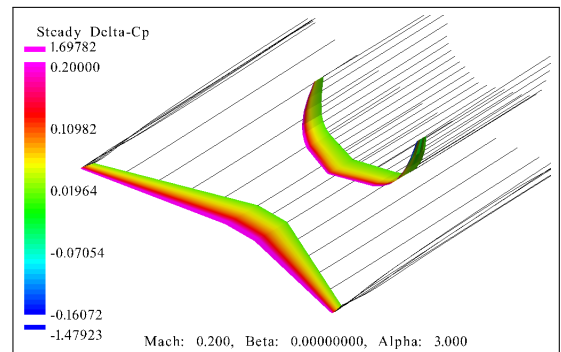
Figure 3.8: *Influence of wing on the empennage*

with the selected airfoil a natural laminar airflow on the lower surface of the wing is achieved.

The usual disadvantage of forward swept wing, the aerodynamic instability, is compensated by an automatic control through increasing the lift coefficient locally by manipulating the boundary suction on the upper side of the wing. The requirements for the electric regulation and compensation circuit are moderate as aircraft of this size have low rotating speeds of less than $3\frac{\circ}{\sec}$. As for the structural instabilities they are compensated by an adequate aeroelastic tailoring, which utilizes the anisotropic twist-bending coupling of the carbon fiber layup. [31].

For the airfoil the CERAS airfoil family is selected to preliminarily estimate lift and drag. In an upcoming iteration an appropriate, supercritical airfoil has to be selected. To further optimize the wing, a dihedral angle of 5° is chosen, while the wing twist is adapted manually. The combination of wing, empennage and fuselage designed as such that the maximum lift coefficient is achieved at cruise, with a moment coefficient of 0.

Coanda Flap

The requirement for a long laminar flow on the wing airfoil in order to reduce drag during cruise prohibits the use of a slat track, as this creates a gap in the airfoil and initiates the laminar-turbulent transition. Nonetheless at low velocities high lift coefficients are necessary for a stable approach. In order to prepare for this challenge, multiple universities, especially the DLR in Braunschweig [32] research on the advantages of Coanda flaps. The Coanda flap uses a small air jet parallel to the airfoil in its aft to control the boundary layer and sustain an attached airflow over the surface and allow higher flap deflections without flow separation. As Coanda flaps have the same geometry as normal flaps, they can be both used for regular flight without blowing air and as lift increasing devices during the approach. The necessary air is partially produced by the fans from the

Figure 3.9: *Function of Coanda-Flap System*

boundary layer control suction system and additionally supplemented by two redundant compressors that are located on the inboard section of the wing and then distributed to the flaps. As the necessary lift coefficient for an approach is $c_{L_{max}} = 2, 8$, a deflection of the flap by 20° is sufficient to allow operation of the aircraft. Nonetheless, as the technology of the Coanda flap is currently in development, the maximum deflection angle is set to 40° with a maximum theoretical lift coefficient $c_{L_{max}} = 3, 2$, a maximum angle of attack of 8.5° with activated system and a technology uncertainty factor of 0,9 used to reduce the estimated lift coefficient. This factor includes possible reductions of lift due to disturbance in the airflow of the wing as the pylons for the engine mounting as well as losses of maximum lift coefficient in order to sustain full rudder functionality. Using this uncertainty factor, the maxim local lift coefficient results to $c_{L_{max}} = 2, 88$ and $c_{L_{max,TO}} = 2, 24$. Takeoff and landing are possible with inoperable coanda system and higher angles of attack, although the distances increase significantly. Additionally, as a minimum of moving parts is used, an decrease in noise pollution resulting form slats can be assumed [33]. In addition, landing approaches with coanda flaps are performed at low angles of attack of around 3° [32] increasing the visibility of the pilots on the runway and increasing the overall safety.

The coanda flap is designed as such, that during cruise, when higher lift coefficients are limited by the onset of buffet the air sucked in by the boundary layer control system on the upper surface of the airfoil can be used during cruise to reduce the induced drag of the airfoil. By ingesting an airflow into the wake of the airfoil a reduction in the viscous dissipation is achieved, reducing the induced airfoil drag by 1% [34].

According to Radespiel [32] a functional coanda flap system the required mass flow equals to $\dot{m} = 6.06375\frac{kg}{s*m}$ totaling in a total mass flow of $206\frac{kg}{s}$. The necessary fan power is approximately 5kW.[35]

Boundary layer control

To reduce disturbances and delay laminar turbulent transition the boundary layer control system sucks in air from the upper surface of the wing. Combined with the forward swept wing and a low cambered airfoil laminar airflows up to 40% of the airfoil are achieved that lead to a drag reduction of 16% [36]. At this point the boundary layer is no longer controlled and transition from laminar to turbulent occurs. The energy necessary to drive the pumps and propellers is diverted form the gas turbines in the rear of the aircraft. Similarly to the contra-rotating open rotors in section 3.1 their revolution speeds are tied to the gas turbine and use the alternating current directly to avoid the disadvantage of inverter losses.
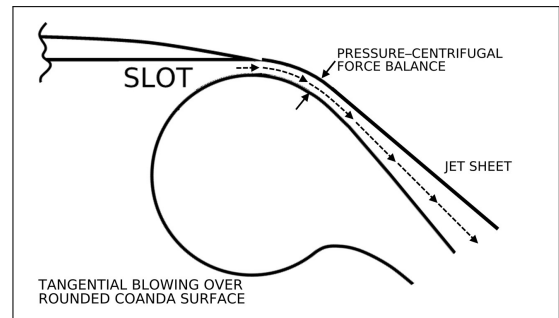
Empennage

The twin tail unit is located directly under the engines and has a continuous transition from horizontal tailplane (HTP) to vertical tailplane (VTP) to reduce drag in flight. Figure 3.8 shows the vorticity distribution at an angle of attack of 3 degrees. As visible, the wing wake does not have an influence on the empennage or the propellers. The trailing wakes at the transition from the HTP to the VTP show that the flow is straight and not disturbed.

In addition to the compensation of the moments generated by the wings, the empennage is also designed to encapsulate the propellers and shield their noise from the downward direction. Due to the long profile in the propeller area, a large part of the generated noise is deflected upwards, thus reducing the noise near the ground. The empennage covers the whole bottom side of the propeller to get an optimal noice shielding, which is shown in figure 4.1. Another advantage of this configuration is that there is no possibility of a shaded VTP through the HTP, which is also shown in figure 3.8.

The fixed tail unit is designed to compensate the arising moments during cruise flight.Therefore, a NACA0012 profile for the whole empennage used.

The size of the VTP is determined by volume coefficient for two loading cases - one with MTOW and one with operating mass empty (OME). According to Raymer [37], the values $V_{VTP,OEW}$=0.041 and $V_{VTP,MTOW}$=0.044 are within the acceptable range for the aircraft class. Because the aircraft has 2 VTP's, each value has to be doubled.

Two additional calculations were made for the moment equilibrium: one in cruise conditions and one for landing or take-off.Since the NACA 0012 profile is symmetrical, no tilting occurs at an angle of attack of 0 degrees which leads to a resulting Moment of 0 Nm.

The the size of the rudder are in the range of about 25% to 30% of the tail chord, which covers an sufficient area according to Raymer [37].
The HTP is calculated with a moment equilibrium for the static longitudinal stability, where the HTP, the wings and the fuselage have to be considered. The centre of gravity of the aircraft is the reference point for the calculation. In this case, the two loading-cases are considered, the OWE and the MTOW. The resulting angle of attack in table 3.2 is calculated with the textbook methods from Raymer [37] and the IFB [38] and the measured lift coefficient for the empennage.

Table 3.2: *resulting α*

Flight attitude	CG	Resulting $c_{L-Empennage}$	Remaining needed $\alpha_{empennage}$ in [°]
Cruise	OME	-0.0549	-0.15
Cruise	MTOM	-0.0495	-0.05
Take off / Landing	OME	-0.10985	3
Take off / Landing	MTOM	-0.09891	2.75

A twist at the HTP root creates an optimal lift distribution and resulting moment around the center of gravity that balances the resultant moment from the wing and fuselage during cruise.To compensate the remaining moments, the elevator is used.

In conventional aircraft designs, the rudder deflection creates a gap between the fixed tail and rudder, which increases turbulences and hence drag. Therefore, the elevators and the rudders consists of the morphing wing technology. The blue dashed areas in figure 3.10 are made by special transition surfaces of monolithic elastic structures, which close the gap between the moving and the static parts [39]. In the morphing rudder, the ribs are driven by the actuator, which leads to a change in the profile. This change in shape is independent in the spanwise direction, resulting in a more adaptable airfoil structure. The fuel consumption is also affected by the new transition areas and the flexible shape of the rudder. In a previous investigation, this technology has already been used to achieve a reduction of the drag coefficient up to 26.73 % and a delay in the transition point of up to 24.81 % [40]. If deployed commercially, aircraft equipped with the morphing wings could see fuel savings of 3 to 4 percent [41].
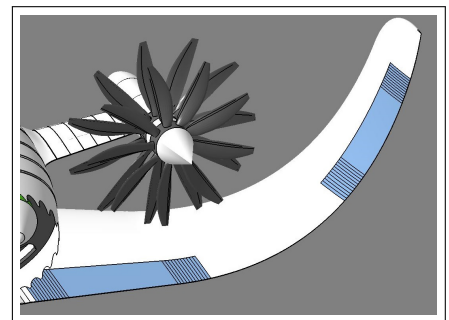
Figure 3.10: *Transition Surface of the morphing Wing*

The elevators are in the range of about 25% of the tail chord, which covers an sufficient area according to Raymer [37].

Aerodynamic Stability

An forward-swept wing aircraft with the propulsion chain located at the aft of the aircraft and low-weight tanks located at the front with close to no additional masses located inside the wing poses a challenge for an adequate aircraft stability design as the center of gravity of the empty aircraft is located in the rear of the aircraft and shifts depending on the amount of passengers and luggage. Contrary to kerosene aircraft, the fuel loss during flight does not significantly change the center of gravity. In the loading diagram (figure 3.11) the stability margin of the aircraft is displayed. The borders of 6 % and 36 % are chosen according to literature [42] and CeRAS [4] regarding comparable current aircraft.
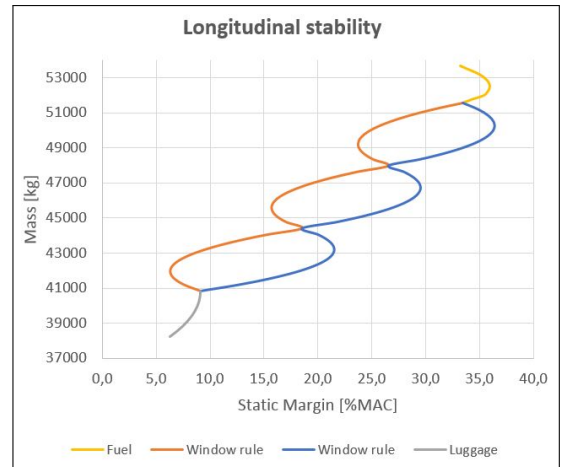
Figure 3.11: *Static margin diagram of Polaris*

4 Design Overview

In general *Polaris* is designed to retain similarities to the CeRAS. With the standard configuration of a low-wing aircraft, standard tailplane and similar dimensions a need of new airport infrastructure is avoided. Nevertheless the design is optimized regarding aerodynamics, propulsion efficiency and a smart integration of propulsion systems. In addition, safety precautions are taken to guarantee a save operation of the aircraft regarding the current certification specification CS25. The three side and an isometric view can be found in figure 4.1.
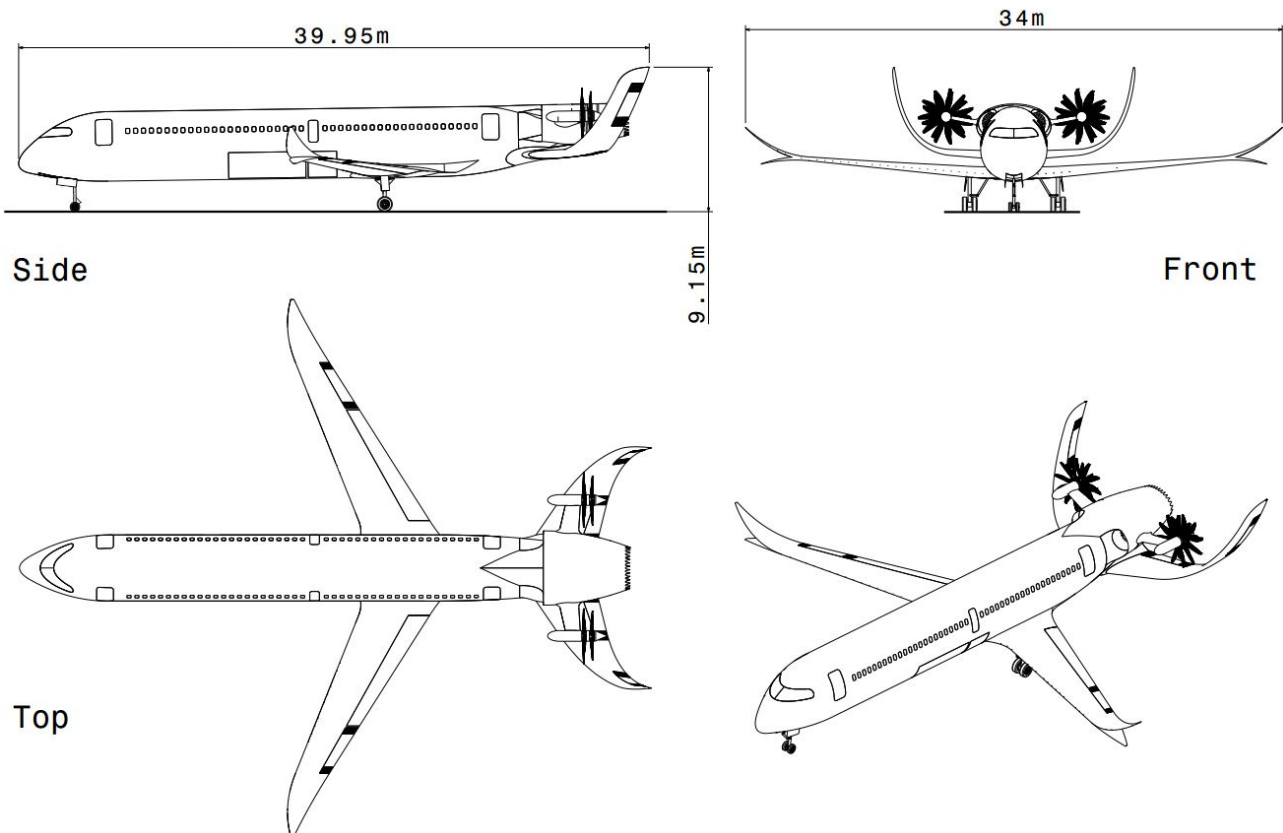
Figure 4.1: *Three side and isometric view*

4.1 Fuselage and Wing

With the use of the Gondola Concept a multi-functional fuselage is designed. In contrast to conventional designs this fuselage is designed with the consideration of storing the fuel tanks, yet locating them outside the pressure cabin. For the maximum fuel volume of $32\,m^3$ most of the space below the passenger cabin is used for fuel storage. For the basic version of the aircraft the fuel system consists of two parallel storage tanks at the front of the aircraft and a pair of feeder tanks between the wing box and the gas turbines. For a long range version of the aircraft two additional tanks can be installed. These optional fuel tanks can be stowed at the cargo area and are connected to the storage tanks in the front. The remaining cargo area remains usable to load cargo containers and is detached from these additional fuel tanks.
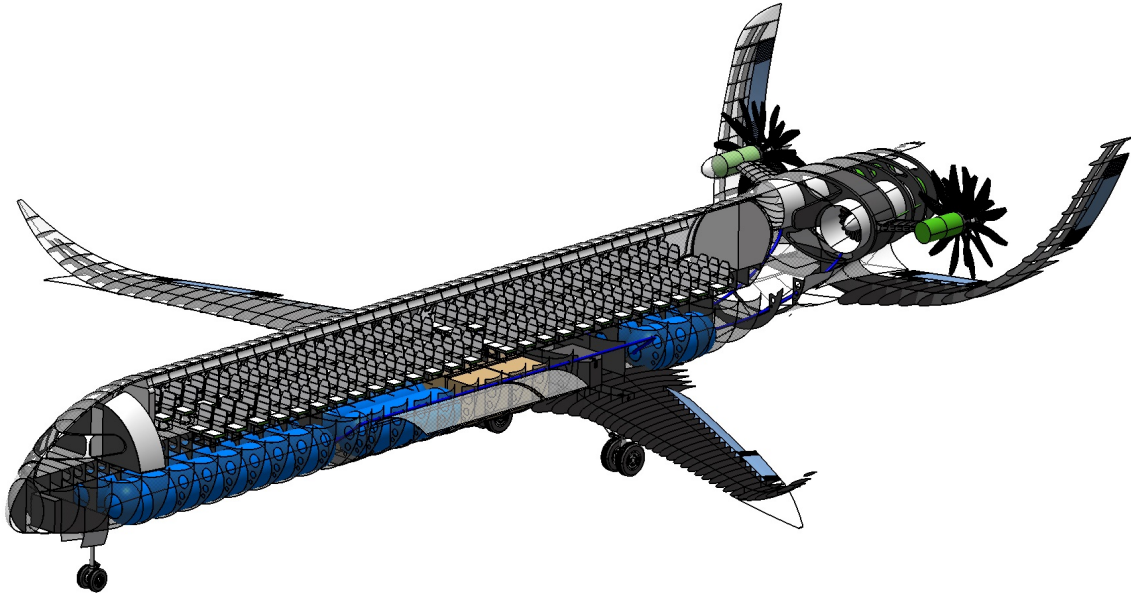
Figure 4.2: *Integration of fuel system, cargo and propulsion unit*

Cabin Layout

The primary structure of the fuselage contains the pressure cabin and therefore includes the cockpit and passenger area. With two entrance doors and a similar cabin layout to the A320, the turnaround time is calculated to last 27 min (cf. section 6.5). Three emergency exits to each side allow a quick evacuation of the passengers in case of emergency. The proposed seat layout includes two classes with a 12-seat business class and a 138-seat economy class.
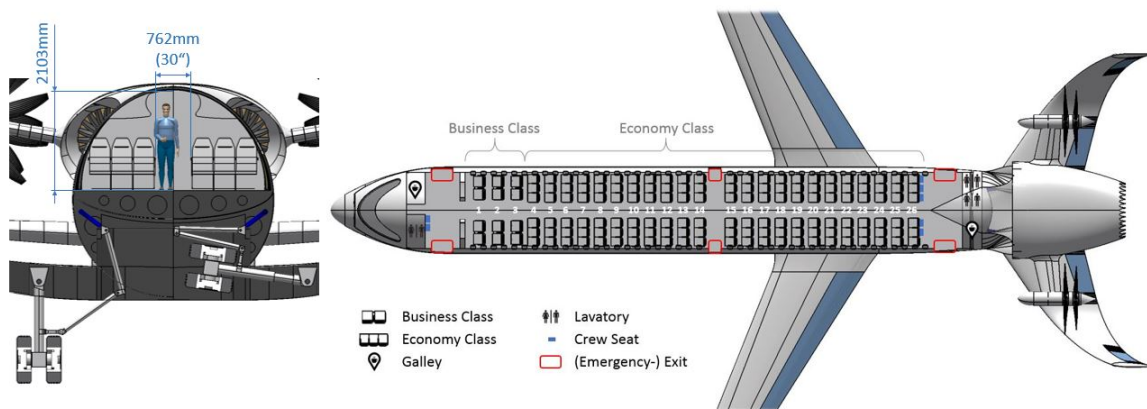
Figure 4.3: *Fuselage Section and Cabin Layout*

4.2 Gear

The aircraft is a conventional-assembly with a twin-wheel configuration. These are designed to hold the aircraft horizontal in both the sprung and unsprung states. The main gear is stored in the wing/fuselage junction. Thus, no additional structure has to be built on the fuselage which would produce aerodynamic resistance and additional mass. Due to the gondola concept, in which the pressurized cabin is placed only in the upper fuselage cross-section, there is enough space in the wing root area for the gear to be placed. Since 90 % of the total mass must be carried by the rear gear [37], it is attached to the fuselage structure with additional reinforcements. The diameter and width of the wheels were calculated using Raymar textbook methods

The gear is placed with a sufficient distance to the rearmost center of gravity in the X direction to avoid tilting backwards.Like the main gear, the nose gear is attached to the structure of the aircraft under the cockpit, where it is additionally reinforced by a specially designed gear box.

4.3 Empennage and Propulsion System
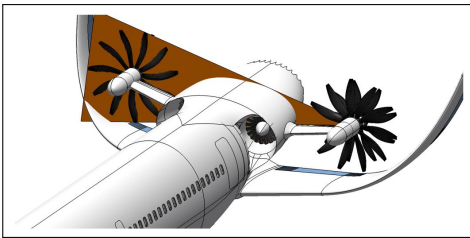
Figure 4.4: *Burstcone CROR*

Contrary to the currently most commonly used gas-turbines, that already have protective nacelles surrounding the rotating parts, additional security measures have to be taken to ensure safety in case of a critical blade failure. Therefore the propellers are mounted in the aft of the aircraft, far away from the passenger cabin. Additionally, as both propellers are close to one another, the rear section of the aircraft was designed as such, that the engines are not in the line of sight of one another and thus a ruptured blade cannot collide with the propeller on the other side of the aircraft.

In the event that the blade hits the morphing wing, only the limited affected area becomes inoperative. The unaffected independent moving parts of the elevator can still be controlled. The empennage is mounted to the main structure under the turbines. The reinforced structure in this area, which is shown in figure 4.5, has sufficient stability that can transmit the moments and forces that occur.
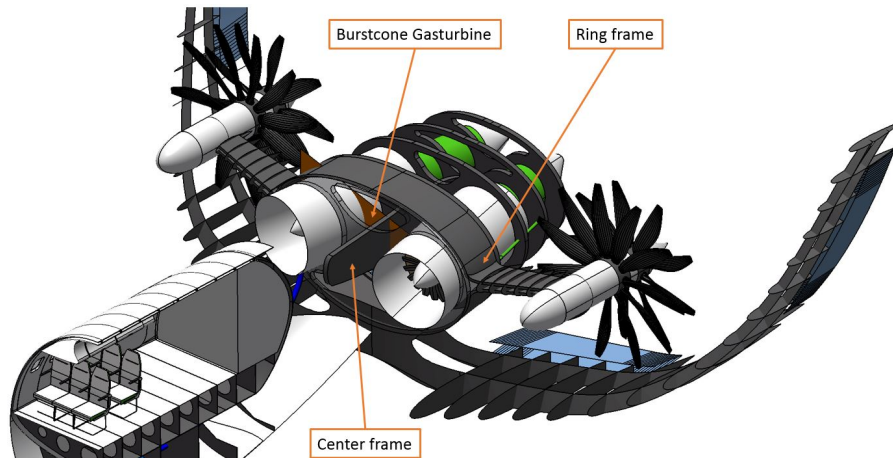
Figure 4.5: *Assembly of empennage, propulsion system and fuselage*

4.4 Fuel System

In comparison to kerosene tanks liquid hydrogen tanks must be able to fulfill more requirements. To the general task of keeping the fuel in its desired place, LH_2 tanks have to keep the hydrogen in a liquid state. This means the inner temperature has to be kept at 21.7 K at a pressure of 1.4479 bar [43].

The tank configuration has next to storage reasons also operational and integrational causes. The final decision can be seen in figure 4.2.

As you can see above we decided to use six tanks. Two of them are always arranged alongside and in a parallel way. If they are fully loaded with 2200 kg, the front tanks carry each 600 kg amount of LH_2. The residual smaller ones carry 250 kg per tank. The segmentation has on the one side operational reasons and on the other hand weight and balance causes. Due to the relatively high impact of the tank weight on the OME, an extra short-range version is planned. Therefore, unnecessary tanks should be removable, in order to convert

the aircraft. The second segmentation has its reason in the position of the wing. Its structure divides the aft tanks into two parts. This results in four smaller tanks. The aft ones close to the engine functions as a feeder tanks whereas the other ones can be removed if this is desired. The main driver for tank configurations are explained in more detailed beneath.

Volume

The basis to an effective tank configuration is to reach necessary storable volume, which is desired for the intended missions. With the known density of liquid hydrogen, this is a fixed value to deal with [44].

Shape

The second driver is the tank's shape. Due to the very low density of LH_2 the integration was the main problem when designing a hydrogen aircraft in the past. The ideal shape to store liquid hydrogen is a sphere because it reduces the surface area, which is the main reason for a high rate of vaporizing hydrogen. Of course, it is not possible to fit all fuel in one sphere. The logical conclusion, when looking at the fuselage is a cylindrical shaped tank. The pressure distribution is not as good, but with two hemispheres closing the cylinder, it is still feasible [44]. With respect to the available space in the fuselage the outer diameter of the cylinder is fixed and with it the resulting length of the tanks, too. Additional improvements can be gained by the use of a dished bottoms instead of the hemispheres. It small disadvantages in terms of surface area but a reduction of the tank's length makes the choice reasonable [45]. Both the cylindrical shape and die dashed bottom help to reach the goal to place the tank in the lower fuselage and are quite easy to manufacture. This has big advantages concerning the aerodynamics compared to other projects which decide to attach them outside the fuselage [44]. There are two basic possibilities to integrate the tank in the fuselage. The chosen one is the non-integral way. Studies say integral tanks only have small weight advantage, which gets smaller if you increase the design life up to the service life of the aircraft [43]. Safety thoughts made the final decision. Damages at the fuselage structure don't follow in a loss of all the fuel if you use non-integral tanks. On top of that they are removable which makes maintenance inspections much more easier and the short-range Version possible.

Insulation

The wall structure of an LH_2 tank is closely linked with to the selection of the insulation material. The chosen material is polyurethane, a from CO_2 frothed up foam. It is easy to handle, cheap and has a low density. Other vacuum-based insulations turn out to be too dangerous in the case of a vacuum loss [44].

The structure can be seen in figure 4.6.

Due to heat transfer effects the stored LH_2 changes phase to GH_2 which can diffuse through the tank wall. That makes the insulation necessary. The amount of diffused hydrogen by time mostly depends on the tank's surface area and on the insulation layer thickness. This amount can be estimated by equations based on [45].

Although it is recommended to leave the hydrogen in the aircraft even on ground over night, it might be possible to defuel when the aircraft is

Figure 4.6: *Insulation layers tanks [46]*

out of service. This might be the case if there is a major maintenance event coming up or the tanks need an inspection them self. Tanks need to be checked every 4000 flight hours. To inspect them from inside the LH_2 has to be removed, purged and filled with breathable air. After defueling and purging there is still GH_2 left in the tanks. The warm up procedure can be started and after reaching 77.6 K the fuel storage can be filled with dry nitrogen gas. This procedure removes nearly all left hydrogen. After flushing them with air to remove the nitrogen, the tank can be entered [43]. Refueling procedure is similar but in reverse order. By nitrogen air and CO_2 are flushed out. Purging the tank from nitrogen is done by GH_2. During that the chill-down process of the tank starts by the use of cold GH_2 . Fueling a warm tank with LH_2 must be conducted slowly at first to avoid over-pressurizing. The flow rate can be increased with decreasing a tank temperature. This whole process must be done over night, to prevent absence form service [43].

Fuel System Safety

In contrast to aircrafts with standard configurations, storing the fuel in the tanks, the hydrogen tanks are located in the belly of the fuselage. This means they are directly placed underneath the cabin. Therefore special considerations have to be made. In case of a damage of the tanks it must be proven that leakage does not interfere with passenger's safety.
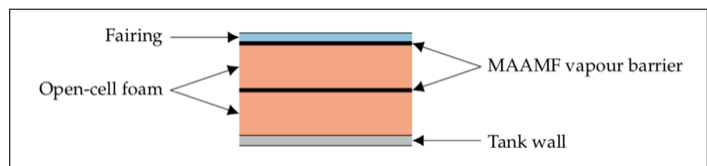
"In most cases a comparison of fuels will show hydrogen to be the safest and least devastating"

    - Bhupendra Khandelwal et al in *Hydrogen powered aircraft : The future of air transport*, January 2013

Releases of LH_2 out of tanks at a rate of $60\,\mathrm{L/min}$ were investigated under conditions of ignited and unignited leakage [47].

The unignited test showed that a pool of liquid and large solid deposits are produced. They kept stable in their phase and disappear after several minutes. Tests with ignition of the vapor above the solid deposit pointed out that a flame emerges but no explosion occurs [47]. In comparison to that kerosene fill out as much space a possible. LH_2 is localized to the leak and vaporising in a controlled way [44].

In the ignited case turned out to be difficult. The clouds of H_2 occurred after the leak of LH_2 is difficult to ignite. The reason may be that the gas cloud is over-rich in hydrogen. In case of an successful ignition the hydrogen burned out in the form of a gentle jet flame from the release point about 1 meter high. It was discovered that hydrogen flames usually radiate less heat than hydrocarbon gases flames. While kerosene burned out in an uncontrolled way endangering the passengers with high risk for loss of lifes, LH_2 is shone to flame out in a very controlled manner. No fire carpet will be formed [44].

Furthermore, flammability tests prove the liquid hydrogen to burn around 14 times faster than kerosene for the same fuel volume. Burning $121\,\mathrm{L}$ of propellant takes $27\,\mathrm{s}$ or $7\,\mathrm{min}$ respectively. The reduced time span will prevent the fuselage to collapse due to high heat levels [43].

4.5 Mass Estimation

One of the keys of every aircraft design project is the estimation of the vehicle's system masses.
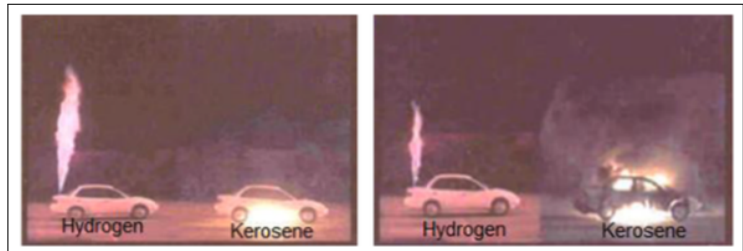
Figure 4.7: *Flammability compared between LH_2 and kerosene [44]*

With empirical formulas it is possible to get a first impression on how the structure, the power unit, the systems and additional furnishings plus operational equipment will affect the OME. A detailed breakdown of all related components of the long range version of *Polaris* can be seen in table 4.1. For the OME the long range version is crucial because it is the critical case in terms of structural loads. The short range version with less tank storage volume is applicable for MTOM and therefore restricts the amount of fuel.

There are plenty of methods to find in the literature. Not each of which suits to the projects aircraft size and type. The first step is to recalculate the reference plane. These results are compared to the actual component weights of CeRAS. For this task the weight estimation approaches of Raymer [37], Torenbeek and the GD method [42] were compared. It shows that the techniques of Torenbeek and the GD method came the real CeRAS weights the closest. It is not recommendable to just use one method. Each has disadvantages in different fields. It is always a good way to take two approaches into account and build the mean value out of them. The best results for the CeRAS recalculation were found by the mean value of Torenbeek and GD.

As a third step the variance of results of the mean values from the actual weights of CeRAS has to be calculated for each component. In total it was successful to reproduce the OME with an accuracy of $-5\,\%$. These variances are added as factors to the mean values of the *Polaris* calculation. This has to be done for each component and results in the final weight of each element of the *Polaris* aircraft. This is also described in figure 4.8.

The new fuselage segmentation was already addressed in chapter Due to the cutting-edge technologies used for the propulsion system, it is not possible has to calculate all components by textbook methods. The data are refereed to 3.1
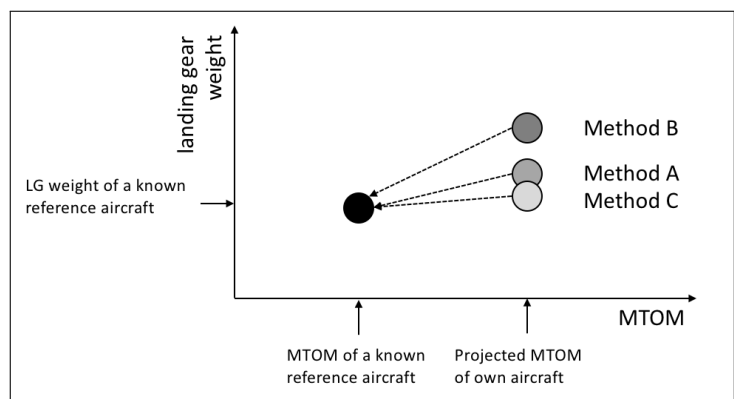
Figure 4.8: *Calibration method of component weights based on [48]*

Table 4.1: *Mass Breakdown of Polaris and CeRAS*

Description	Unit	*Polaris* Value	CeRAS Value
Max. Take-off Mass (MTOM)	kg	**53993**	**77000**
Max Zero Fuel Mass (MZFM)	kg	**51967**	**62100**
Operating Mass Empty (OME)	kg	**37967**	**42092**
Manufacture's Mass Empty (MME)	kg	**33542**	**38153**
STRUCTURE	kg	**17206**	**22018**
Wing	kg	7054	8097
Fuselage	kg	5722	8986
Horizontal tail	kg	809	682
Vertical tail	kg	723	522
Landing gear	kg	1781	2491
Pylons/Nacelle	kg	1117	1239
POWER UNIT	kg	**9185**	**7751**
Equipped engine	kg	1950	7520
Electric Motor	kg	2200	-
Generator	kg	2200	-
Propeller	kg	78	-
Air induction system	kg	477	-
Power Cable	kg	120	-
Tanks	kg	1547	-
Engines control	kg	39	n/a
Fuel system	kg	573	231
SYSTEMS	kg	**4306**	**5378**
Auxiliary Power Unit	kg	-	292
Hydraulic generation & distribution	kg	627	899
Air conditioning	kg	780	739
De-icing			42
Fire protection	kg	92	92
Flight controls	kg	456	799
Instruments	kg	886	85
Auto flight system			139
Navigation			565
Communication			277
Electric generation & distribution	kg	1466	1449
FURNISHING	kg	**2846**	**3006**
OPERATOR ITEMS	kg	**3955**	**3939**

Electric Motors, Generators and Power Cables

Electric motors and generators are characterized
by a power density of 20 kW/kg. With the supplied electric power of 22 MW, electric motor and generator weight 1100 kg per unit. See 3.1.

The mass of the transmission lines can be reduced because they are designed as superconductors. This results in a specific cable mass of 10 kg/m [49]. With considering cross-feeding of the EM the length is estimated with 12 m. This results in 120 kg for the power cables. See 3.1.

Tanks

How LH_2 tanks are built is already described in chapter 4.4. The weight results out of the density of the materials and the calculated volume of tank structure, the isolation layer and anti-slosh walls. Because degassing also depends on the amount of LH_2 carried in one Tank, the layer thickness might differ between the two used tank sizes. A detailed breakdown of the calculation of the insulation layer can be found in [45]. The fairing and MAAMF vapor barrier are so light that they do not need to be considered. An overview about the mass of the single components can be found in table 4.2. The long range version inhibits two small tanks more, so this is the version crucial for OME.

Table 4.2: *Tank component weights*

Component	Unit	Value	
		Small Tank	Large Tank
Structure		126	281
Insulation layer		50	112
Anti-slosh wall	kg	7	14
Single Tank		183	407
All Tanks		1547	

Fuel delivery lines

The fuel system contains of fuel delivery lines and pumps. A pump weights 28,8 kg. With one pump for every tank this leads to 514.8 kg in total [43]. The mass of the delivery lines was calculated by the densities of the used material. Their structure can be seen in 4.9. Just like the tanks it is important to bring the degassing effect to a minimum. With an estimated way of 25 meters the delivery lines weight 54.3 kg [43].

The Inconel 600 is used due to the the problem of hydrogen embrittlement. This is mainly an issue for the delivery lines. Steel and titanium are often affected by this problem. Ni-Cr based alloys show similarities to austenitic steels build the exception from the rule. They are already used in space flight for cryogenic cooling of engine nozzles [50] [51].
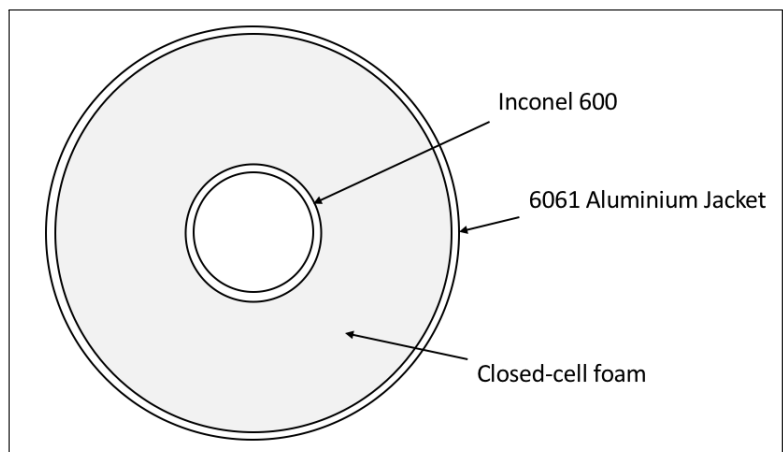

Figure 4.9: *Cross section of fuel delivery lines based on [43]*

4.6 Technology Readiness Levels

Table 4.3 shows a summary of the used technologies with their current technology readiness levels.

Table 4.3: *Technology readiness level*

	Technology	TRL	Source		Technology	TRL	Source
Propulsion System	Intercooler	5	[52]	Aerodynamics	Morphing Wing	7	[41]
	Recuperator	4	[52]		Coanda Flap	4	[32]
	HTS-Technology	4	[53]		Active Laminar Flow Control	7	[36]
	Low Noise CROR	6	[5]				
	Advanced Combustion	4	[54]		Riblet Surface	5	[25]
	LH_2 Fuel Tank	8	[45]		Gondola-Fuselage Concept	6	[23]

5 Aircraft Performance

Mission Calculation

To determine the saved energy of a new aircraft design an accurate calculation of the fuel consumption for both the reference aircraft and the new design is required. The CeRAS database offer calculations for three different missions, each containing detailed information about the fuel for mission segments and reserve fuel. A high level of comparability is achieved by choosing the CeRAS mission profile, shown in figure 5.1, for *Polaris*. Consequently, this allows to easily integrate the new aircraft into the current flight planning structure. Changes are made in the design range and cruise Mach-number, as described in chapter 1 and section 3.1.

The mission calculation consists of three segments each for the 1500 NM design mission and a 200 NM diversion flight.

To account for the changing air density and drag, the climb distance from sea level to cruise altitude of 35 000 ft is split into steps of 5000 ft utilizing the corresponding environmental data, aircraft mass at the beginning of each segment, lift-drag-polar and engine power output. The cruise flight is then computed using the Breguet equation. Finally the descent is calculated in the same manner as the climb phase, while being performed at the point of best glide. The overall distance is then calculated as the sum of the distance flown in each segment. Table 5.1 shows the relevant data of the design mission.

In a next step towards an accurate representation of the fuel consumption, the CeRAS mission is modeled using the provided 2500 NM and the 2750 NM data to tweak the mission calculation ac-

Figure 5.1: *1500 NM design mission profile of Polaris*

cordingly, until an accuracy of >99 % is met. This ensures the calculated saving to be as correct as possible. Since there is no data available for a mission with design payload and a range of 1500 NM, the take-off mass and mission fuel is calculated with the previously calibrated model. An additional comparison point exists in form of a study mission with the design payload and a range of 500 NM. Since CeRAS is burning conventional Jet A-1, while *Polaris* is burning LH_2, two different energy densities have to be multiplied with their respective fuel masses to create a comparable energy value. The results can be seen in table 5.2. A total energy saving of 61.59 % is achieved for the design mission, which meets the goal of >60 % previously set. On shorter ranges the difference is greater, since the weight reduction due to fuel burn is of minor importance.

Table 5.1: *Mission calculation data for the* 1500 NM *design mission of the Polaris concept*

Climb:	Unit	Value	% of mission
Fuel	kg	219.40	15.94%
Energy	MJ	26 327.98	15.94%
Time	s	1 115.29	8.40%
Energy consumption	MJ/s	23.61	-
Distance	NM	102.60	6.84%
Average climb rate	ft/min	1 613.93	-
Cruise:			
Fuel	kg	1 134.68	82.45%
Energy	MJ	136 162.17	82.45%
Time	s	11 253,33	84.79%
Energy consumption	MJ/s	12.10	-
Distance	NM	1 326.29	88.39%
Cruise speed	ft/min	776.10	-
Cruise altitude	ft	35 000.00	-
L/D	-	20.23	-
Descent:			
Fuel	kg	14.81	1.08%
Energy	MJ	1 777.77	1.08%
Time	s	903.11	6.80%
Energy consumption	MJ/s	1.97	-
Distance	NM	87.91	5.86%
Average descent rate	ft/min	-1 993.38	-
Total:			
Fuel	kg	1 376.24	100.00%
Energy	MJ	165 148.98	100.00%
Time	s	13 271.73	100.00%
Energy consumption	MJ/s	12.44	-
Distance	NM	1 500.46	100.00%

Table 5.2: *Comparison between CeRAS and Polaris for two different mission ranges and the resulting energy saving taking the two different fuel types into account*

| 1500 NM		Polaris	CeRAS	Saving
Trip Fuel	kg	1 376.24	9 038.94	
Trip Energy	MJ	165 148.98	386 866.52	**57.31%**
Reserve Fuel	kg	261.70	2 918.50	
Reserve Energy	MJ	31 404.38	124 911.80	**74.86%**
Total Fuel	kg	1 637.94	11 957.44	
Total Energy	MJ	196 553.36	511 778.32	**61.59%**

500 NM		Polaris	CeRAS	Saving
Trip Fuel	kg	504.53	3 765.00	
Trip Energy	MJ	60 543.19	161 142.00	**62.43%**
Reserve Fuel	kg	261.70	2 900.00	
Reserve Energy	MJ	31 404.43	124 120.00	**74.70%**
Total Fuel	kg	766.23	6 665.00	
Total Energy	MJ	91 947.61	285 262.00	**67.77%**

Long-Range Version

In section 4.4 it is mentioned, that there is the option to equip two extra fuel tanks in the lower middle fuselage to achieve an extended range. In return this limits the maximum payload, both in volume and mass. This reduces the maximum payload mass from 14 969 kg to 14 000 kg, which is the equivalent of 10 passengers. Due to the high energy density of LH_2, this reduction increases the range by a significant amount, as seen in the payload-range-diagram in figure 5.2.

Moreover the diagram shows the low impact of fuel mass in exchange for payload. The additional structural mass of the fuel tanks of 366 kg, is added to the empty mass of the aircraft, which has a negative impact on the efficiency of the long-range version in short range operation. At the design mission this difference is 0.56 %.
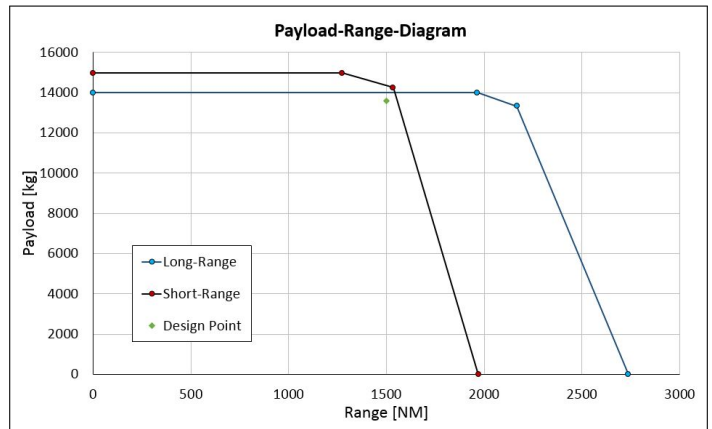
Figure 5.2: *Payload-range-diagram of the short-range and the long-range version of Polaris*

Take-off and Landing

The performance data is completed by take-off and landing calculations. In case of an engine failure after the decision speed v_1 take-off has to be continued. Therefore v_1 is calculated as the speed at which the breaking distance is equal to the required distance of a continued take-off with one engine. Moreover it is considered that the climb gradient with one engine inoperative may not be less than 2.4 % for two-engined airplanes [55]. For the landing distance a reserve of 2/3 is added as required by the FAR to account for different pilot skills. Both field lengths are within the requirement of 2200 m as specified in the TLARS in table 1.1. Similarly to CeRAS the gas turbine power is sized bigger than minimum requirements demand to provide a better climb performance. Table 5.3 contains the calculated values for take-off and landing.

Table 5.3: *Calculated take-off and landing data for Polaris at MTOM*

Take-Off				Landing		
Take-Off Field Length	m	972.48		Landing Field Length	m	1112.86
Balanced Field Length	m	1428.43		Including 2/3 Reserve	m	1854.76
v_1	kts	104.54		Approach Speed	kts	131.01
$v_{s,TO}$	kts	121.88		$v_{s,LDG}$	kts	106.52
$c_{L,max,TO}$	-	2,20		$c_{L,max,LDG}$	-	2.88
				$\gamma_{approach}$	deg	3.00

5.1 Compared key data of Polaris and CSR-01

Table 5.4: *Compared key data of Polaris and CeRAS*

Performance parameter			
Parameter	Unit	Polaris	CeRAS
MTOM	kg	53 993	77 000
MZFM	kg	51 967	62 100
Fuselage length	m	39.95	37.49
Balanced field length	m	1 428	2 184
Landing distance limit	m	1 112.86	1 513
Rate of Climb	ft/min	1 613.9	3 697.5
Cruise Mach number	-	0.72	0.78
Cruise altitude	ft	35 000	35 000
L/D (Cruise)	-	20.17	17.43
$C_{L,max,TO}$	-	2.20	2.20
$C_{L,max,LDG}$	-	2.88	2.80
Wing area	m^2	100.0	122.4
Aspect ratio	-	12.6	9.48
Wing span	m	34.0	34.1
Total fuel consumption (1500 NM)	kg	1 638	11 957
Energy consumption (Climb)	MJ	26 328	43 787
Energy consumption (Cruise)	MJ	136 162	346 551
Energy consumption (Descent)	MJ	1 778	2 528
Energy consumption (Reserve)	MJ	31 404	124 912
Total energy consumption (1500 NM)	MJ	196 553	511 778

6 Impact on Operation

6.1 Pollutant Emissions

A secondary goal for the design apart from efficiency is the reduction of pollutant emissions and NO_x in particular, for which the IATA set the target of -80% [2]. To achieve this, a mixture of technological and operational adoptions has to be applied.

The use of LH_2 brings both positive and negative side effects. Contrary to carbon based jet fuels, whether Jet A-1 or biofuels, liquid hydrogen does not produce carbon monoxide (CO), carbon dioxide (CO_2), soot or particulate matter (PM). The only pollutant emissions of a LH_2 flame are water vapor and NO_x. This means the design of the combustion chamber does not have to balance between CO, soot and PM on the one side and NO_x on the other, as it has to with current combustors. Therefore an optimization solely for NO_x can be done. As a measure for this LH_2 can be burned at a much leaner fuel to air ratio than kerosene, which in turn decreases the NO_x production [56]. Significantly lower NO_x emissions can be achieved using the premixing technology "micromix", developed by the FH Aachen. Tests showed a reduction of 77.6% in NO_x emissions compared to a kerosene engine, with simulations predicting an average of 75% for selected gas turbines [57]. Alongside the decreased fuel burn resulting from the efficiency gain of the IRA cycle, described in section 3.1, a reduction of at least 80% NO_x emissions should be possible.

One prominent argument against LH_2 fuelled airplanes is that the combustion of hydrogen produces 2.6 times the amount of water compared to kerosene of the same energy [56]. This water could then go on to form contrails and cirrus clouds, which are reportedly contributing to global warming. While it is acknowledged that aircraft emissions contribute to the formation of contrails and cirrus clouds, the correlation exists primarily because of the amount of condensation nuclei in the exhaust gases [58]. In particular soot encourages the formation of ice crystals making the resulting clouds optical thicker than natural cirrus formations, which results in a higher effect on global warming [59].

During the combustion of hydrogen neither soot nor sulphuric acid is produced. Hence there are less condensation nuclei in the exhaust jet of a LH_2 fueled aircraft. In simulations this results in optical thinner clouds, which have a smaller effect on climate change [56]. To summarize even though there is more water produced by hydrogen combustion, its environmental impact is expected to be less significant.

6.2 Alternative Missions

Additionally to technological optimization, the flight mission can be optimized for different aspects as well. For example the environmental impact of the emissions is greatly dependent on the altitude. This is because the residence time of the respective species in the troposphere is with days to weeks much lower than in the stratosphere with months to years [58]. Therefore to reduce the greenhouse effect of the emissions a lower flight level may be used, see figure 6.1.

To compare the effect on mission duration and fuel consumption a study mission with a cruise altitude of 9000 m was calculated. The results, in table 6.1, show that 25 kg additional fuel are required. This of course diminishes the gain in total fuel efficiency compared to the CeRAS, however, under the premise, that the greenhouse effect of this mission is noticeably smaller it might be worth the trade off.

Figure 6.1: *Comparison of greenhouse effects depending on flight altitude [60].*

Furthermore the greenhouse effect of contrails is largely dependent on local atmospheric circumstances, as is their formation. It may vary greatly from the global mean, both positively and negatively, even to the extend, where the contrails have a cooling effect. With the knowledge of these regional properties, an advanced flight planning concept may be used to circumnavigate the areas where contrails have a warming effect, while deliberately navigating through regions where the contrails cool the local climate.
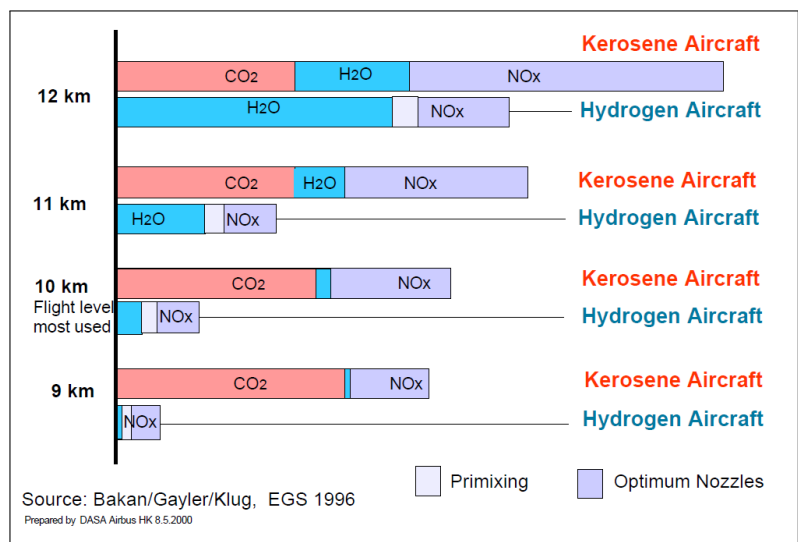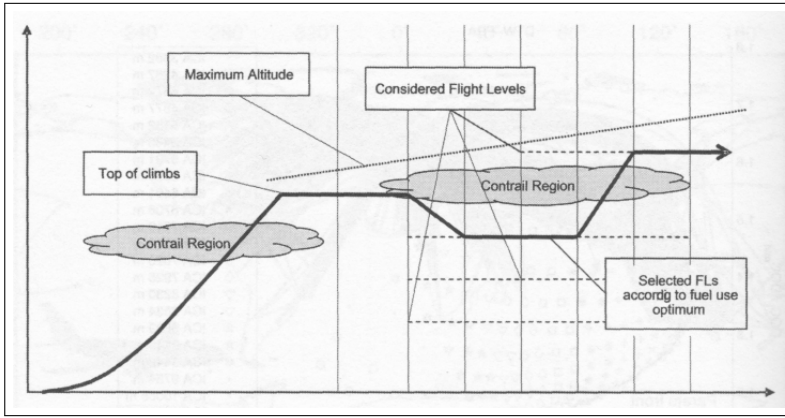
Figure 6.2: *Example on how to optimize the flight path for a smaller greenhouse effect [61].*

By this the impact of aviation on climate might be mitigated [62]. Even though the prospect of nearly climate neutral flight is tempting, additional research on contrails and the impact of hydrogen engines is necessary for a better prediction of the effects on climate change.

A different view on the optimal mission might be the flight time, especially the airlines are interested in as many flights per day as possible. For this the cruise speed should be as high as possible. However as a part of the striving for maximum efficiency, the cruise Mach number has been reduced from $Ma = 0.78$ of the CeRAS to 0.72 due to the optimal working range of the CRORs, see section 3.1. This of course means longer flight times, but it remains to identify how big of an impact that has.

The flight time of *Polaris* for the design mission of 1500 NM is 221 min, which is 19 min more than the calculated flight time of the *CERAS* for the same mission. For comparison an alternative mission for *Polaris* is calculated with an increased Mach number of 0.75 at the cost of a by 6 % reduced propulsion efficiency, according to values given by Torenbeek [7]. This results in flight time reduction of 7.5 min, however at the cost of 115 kg fuel, see table 6.1. The benefit of shorter travel time does not justify the higher fuel consumption, especially if, like for this design, the focus lies on energy efficiency.

Table 6.1: *Calculated data of alternative missions. Note that the fuel consumption at $Ma = 0.75$ exceeds the fuel capacity of the short-range version, so the long-range has to be used in this case.*

		Design Mission	**9000 m**	**Ma = 0,75**
Trip Fuel	kg	1 376.24	1 401.31	1 491.06
Trip Energy	MJ	165 148.98	168 157.55	178 927.14
Energy Difference	%	0.00 %	1.82 %	8.34 %
Trip Time	min	221.20	221.15	213.73
Time Difference	%	0.00 %	−0.02 %	−3.37 %

6.3 Flight related aspects

When climbing with a conventional aircraft the changing pressure is not a problem, because the tanks are vented. Using LH_2 tanks the air cannot be allowed to leave and enter. On the one hand it freeze immediately. On the other the loss of fuel due to diffusion would rise strongly. In consequence of this problem tanks must be airtight and designed to a constant overall pressure [43]. The tank's structure cannot prevent diffusion in total, so you need total calculate the amount of LH_2 that will get lost during flight [45]. According to that on a 3 hours flight about 50 kg fuel cannot be used due to diffusion if the tank is fully filled up. This is about 2.2 % of the tanked mass.

6.4 Airport Modifications

Modifications of airport equipment for cryogenic hydrogen are possible. It is economical feasible to locate liquefaction plants directly at the airport. Especially LH_2 lends oneself to feed every parking position directly without the use of fuel trucks. An airport fuel transfer system feeds each parking position. The use of fuel trucks is possible, but the boil-off rate is higher [43]. LH_2 maintenance hangers need vents in their roofs for removal of hydrogen vent gas. On top of that defueling and refueling after checks take quite some time. This means special facilities will be needed for that [43].

6.5 Groundhandling and Turnaround

For most economical flight a minimization of the turnaround time is required. NASA's N+3 goals state, that in 2050 99% of all flights should have a turnaround of less than 30 minutes [63]. In the following a turnaround time is estimated with respect to the Polaris. Due to the size of the aircraft and the number of passengers, it is assumed that the aircraft is allocated a parking position at the gate. Tasks during this time include deboarding and boarding of the passengers, loading the four containers, cleaning, restocking the catering and refueling the aircraft.

Passenger boarding and deboarding can be performed using both doors. In accordance to Scholz [64] deboarding of 30 passengers per minute and boarding rates of 18 passengers per minute are achieved. Simultaneously containers can be loaded and unloaded with a rate of 1,5 Containers per minute [65].

In accordance to Brewer [43], for refueling 10 minutes are calculated, consisting of the attachment and detachment the LH_2 fuel adapter (2min each), the refueling process with a flow rate of 20kg/s (1min) and purging as well as chill-down operations (5min). These high flow rate can only be achieved by using a specially designed fuel adapter introduced by Brewer.

For catering 7 min and for cleaning 8 min are allocated. [66]. Therefore the whole process needs 27 min and is displayed in 6.3.

In figure 6.3 a possible ground-handling procedure is presented. It shows, that all involved vehicles have enough space to fulfill their task in their allocated times. A special focus should be taken with fuel trucks on the left side of the aircraft. In this design two fuel trucks are placed alongside the left wing. Both are necessary due to the segregation of the fuel system in a left and right side. On the other side of the aircraft, the used unit load device (ULD) loader has to be fully movable and equipped with a hydraulic ramp due to the limited space concerning the forward swept wing. The load has to pick the container up because the ULD transporter cannot park close to the aircraft.

In additional boil-off aspects have to be considered on ground too. If the aircraft remains on ground for a long time, for example overnight, some of the LH_2 stored in the aircraft will get lost. The calculations for 12h tell that in this time 201.56 kg of fuel diffuse.
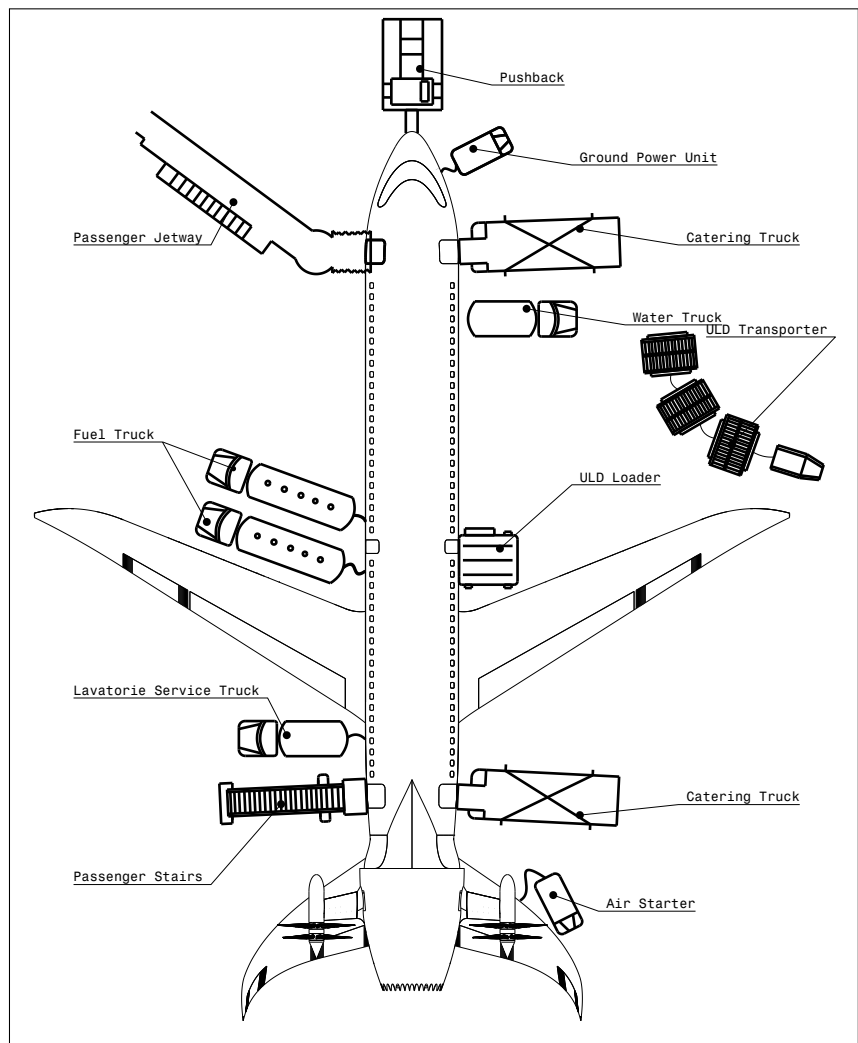

Figure 6.3: *Ramp Layout of Polaris*

7 Summary

The present report shows an aircraft design with its considerations, decisions and benefits resulting in *Polaris*, that matches future aviation goals. While the main objective is to drastically reduce the energy consumption of a reference aircraft, design decisions are made due to this task. Furthermore *Polaris* considers future goals by decreasing the pollutant and noise emissions, allowing the aircraft to be operated in a similar design mission as an A320 while fulfilling the IATA goals of 2050.

The design process describes the comparison of different propulsion systems and aircraft architectures that might lead to a complete and highly efficient aircraft configuration. Due to the fact that an aspired reduction of the energy consumption cannot be accomplished by optimizing single components of the aircraft, it is about to find the advantages of all components that result in a completed form of synergy. As shown in figure 2.2 the five layers include propulsion systems, fuel types and aircraft configurations with an overlap to design the most efficient design of a future single-aisle transport aircraft.

Chapter 3 presents the key technologies that ensure the improved reference aircraft. Except for high temperature superconducting (HTS) materials all other used technologies are at least tested on a demonstrator or available for series production by now. HTS materials attain technology readiness level 4 while illustrating that the used key technologies of *Polaris* are about to be available before 2025.

The aircraft configuration with its structural components, estimated weights and particularly designed components is shown after the functional description of the key technologies. With special attention to the liquid hydrogen fuel system, all the regarded advantages, challenges and synergies of the design aircraft are presented.

After the recalculation of the reference aircraft in relation to energy consumption, weight estimation and aerodynamics, validated calculation methods are used to evaluate the same values for *Polaris*. As the calculation methods emulate the reference aircraft with a deviation of less than 1%, *Polaris'* results have the same accuracy. In chapter 6 impacts on the operation are compared with their possibility to gain further reductions of the energy consumption and or pollutant emissions. With H_2O and NO_X as only emissions, several options are discussed to handle the future emission goals. Alternative missions, airport modifications and ground-handling illustrate the high integrability of *Polaris* as only insignificant changes are required to operate the design aircraft. With fulfilled future aviation goals it can be demonstrated that single-aisle transport aircrafts do not necessarily need a significantly changed airport or airspace infrastructure. Looking at the aviation in 2045 a competitive operation of aircrafts is not only depended on highly efficient aircrafts but also depends on passenger comfort, manufacturing effort and an excellent life cycle.

Considering the extended requirements *Polaris* combines results, options and discussed challenges to present an aircraft design study for single-aisle transport aircrafts. According to the reference aircraft A320 the energy consumption is reduced by 61.39 %. Furthmore a multi-functional fuselage and a highly efficient propulsion system minimize the manufacturing effort and maximize the reliability and passenger safety.

Bibliography

[1] statista: *Number of yearly flights (world wide)*. 2018. URL: https://de.statista.com/statistik/daten/studie/411620/umfrage/anzahl-der-weltweiten-fluege/.

[2] DLR: *Ausschreibung NASA/DLR Challenge 2018*. 2018. URL: https://www.dlr.de/dlr/desktopdefault.aspx/tabid-10997/1778_read-25601#/gallery/29458.

[3] Gerber, Markus: *Fernweh.com*. 2018. URL: http://flughafen.fernweh.com/detail/info.php?iata=HAM&topic=Durchschnittliche+Flugzeiten.

[4] Aachen, RWTH: *Central Reference Aircraft data System*. 2018. URL: https://ceras.ilr.rwth-aachen.de/trac/wiki/CeRAS/AircraftDesigns/CSR01.

[5] General Electrics, NASA ; FAA: *Open Rotor Engine Aeroacoustic Technology*. 2013.

[6] Hepperle, Martin: *Electric Flight – Potential and Limitations*. 2012. URL: https://www.mh-aerotools.de/company/paper_14/MP-AVT-209-09.pdf.

[7] Torenbeek, Egbert: *Advanced aircraft design: conceptual design, analysis, and optimization of subsonic civil airplanes*. Aerospace Series. Chichester: John Wiley and Sons, Ltd., 2013.

[8] Walther, Rainer: *Verbrennungsprobleme der Luft- und Raumfahrttechnik*. Stuttgart, Universität, Fakultät für Luft– und Raumfahrttechnik, Institut für Thermodynamik der Luft- und Raumfahrttechnik, Skript zur Vorlesung, 2017.

[9] Wilfert, Günter et al.: *New Environmental Friendly Aero Engine Core Concepts*. 2018.

[10] Rick, Hans: *Gasturbinen und Flugantriebe Grundlagen, Betriebsverhalten und Simulation*. Springer Vieweg, 2013.

[11] Boggia, Stefan ; Rüd, Klaus: "Intercooled Recuperated Gas Turbine Engine Concept". In: *41st AIAA/ASME-/SAE/ASEE Joint Propulsion Conference and Exhibit* (2005).

[12] Schmidt, Florian: "Abschlussbericht ILA". In: *REVAP Abschlussveranstaltung* (2014).

[13] Leichtfuss, Sebastian ; Schmid, Gregor: "Arbeitspaket Brennkammer-Turbine-Interaktion". In: *REVAP Abschlussveranstaltung* (2014).

[14] Beschorner, Andre ; Vogeler, Konrad ; Voigt, Matthias: "Probabilistische Analyse Revolutionärer Kreisprozesse". In: *REVAP Abschlussveranstaltung* (2014).

[15] Felder, James L ; Kim, Hyuan Dae ; Brown, Gerald V: "Turboelectric Distributed Propulsion Engine Cycle Analysis for Hybrid-Wing-Body Aircraft". In: AIAA Aerospace Science Meeting; 5-8 Jan. 2009; Orlando, FL; United States (2009).

[16] Haran, Kiruba et al.: "High power density superconducting rotating machines-development status and technology roadmap". In: *Superconductor Science and Technology* 30.12 (2017). URL: http://stacks.iop.org/0953-2048/30/i=12/a=123002.

[17] Radebaugh, Ray: "Cryocoolers for aircraft superconducting generators and motors". In: *AIP Conference Proceedings* (2012), pp. 171–182. URL: https://aip.scitation.org/doi/abs/10.1063/1.4706918.

[18] Masson, P J et al.: "HTS machines as enabling technology for all-electric airborne vehicles". In: *Superconductor Science and Technology* 20.8 (2007). URL: http://stacks.iop.org/0953-2048/20/i=8/a=005.

[19] Berg, F et al.: "Cryogenic system options for a superconducting aircraft propulsion system". In: *IOP Conference Series: Materials Science and Engineering* 101.1 (2015). URL: http://stacks.iop.org/1757-899X/101/i=1/a=012085.

[20] DelRosario, Ruben: *A Future with Hybrid Electric Propulsion Systems: A NASA Perspective*. NASA Glenn Research Center, Cleveland, OH United States. URL: https://ntrs.nasa.gov/search.jsp?R=20150000748.

[21] NASA: *The Promise And Challenges Of Ultra High Bypass Ratio Engine Technology and Integration*. 2011. URL: https://www.hq.nasa.gov/office/aero/pdf/asm_presentations_promise_and_challenges1.pdf.

[22] NASA: *Open Rotor Computational Aeroacoustic Analysis with an Immersed Boundary Method*. 2011. URL: https://ntrs.nasa.gov/archive/nasa/casi.ntrs.nasa.gov/20160004676.pdf.

[23] Luft- und Raumfahrttechnik, Deutsches Zentrum für: *Realization Composite Fuselage Structures under the Consideration of Concurrent Engineering*. 2002.

[24] Grzeschik, Marc: *Materials and manufacturing methods in aerospace engineering*. 2017.

[25] Mayer, Bernd ; Stenzel, Volkmar ; Peschka, Manfred: *Strömungsgünstige Oberflächen durch innovatives Lacksystem-Haifischhaut für Grossbauteile*. 2012.

[26] 2018. URL: `http://www.xflr5.com/xflr5.htm`.

[27] DLR: "Forward Sweep - A Favorable Concept for a Laminar Flow Wing". In: *AAIA/AHS/ASEE Aircraft Design, Systems and Operations Meeting 1988* (1988).

[28] Lutz, Thorsten: *Flugzeugaerodynamik*. Stuttgart, Universität, Fakultät für Luft– und Raumfahrttechnik, Institut für Aerodynamik und Gasdynamik, Skript zu Vorlesung und Seminar, 2012.

[29] Kruse, Martin et al.: "A Conceptual Study of a Transonic NLF Transport Aircraft with Forward Swept Wings". In: *American Institute of Aeronautics and Astronautics* (2012).

[30] Hepperle: *MDO of Forward Swept Wings, KATnet II Workshop*. 2008.

[31] Blasi, L. et al.: "The Twist-Bending Behavior of Forward Swept Wings: A Case Study of a Glass/Carbon Hybrid Composite Structure". In: *Macromol. Symposium,2007* (2007).

[32] Radespiel, Rolf ; Burnazzi, Marco: *Fundamentals in Coanda Flap Design*. 2011.

[33] Khorrami, Mehdi R.: "Understanding Slat Noise Sources". In: *ComputationalAerocoustics: From Acoustic Sources Modeling to Far-Fied Radiated Noise Prediction, Colloquium EUROMECH 449, December 9-12 2003, Chamonix, France* (2003).

[34] Pandya, Shishir A.: *The D8 Aircraft: An Aerodynamics Study of Boundary Layer and Wake Ingestion Benefit*. 2015.

[35] Toolbox, Engineering: *Fan Power Consumption*. 2018. URL: `https://www.engineeringtoolbox.com/fans-efficiency-power-consumption-d_197.html`.

[36] Beck, Nils et al.: "Drag Reduction by Laminar Flow Control". In: *Energies 2018* (2017).

[37] Raymer, Daniel: *Aircraft Design: A conceptual approach*. Education Series, 1992.

[38] Strohmayer, A.: *FE I Teil 4 - SS17 - Handout Auslegung der Hauptkomponenten*. 2017.

[39] Inc., 2018 FlexSys: *FLEXIBLY ENGINEERING THE "IMPOSSIBLE"*. 2018. URL: `https://www.flxsys.com/`.

[40] Gabor, Oliviu Sugar ; Koreanschi, Andreea ; Botez, Ruxandra Mihaela: "Low-speed aerodynamic characteristics improvement of ATR 42 airfoil using a morphing wing approach". In: *IECON 2012 - 38th Annual Conference on IEEE Industrial Electronics Society* (2012).

[41] Olson, Eric: *Morphing Wing Created Using Smart Materials and Actuators*. 2018. URL: `https://insights.globalspec.com/article/7578/morphing-wing-created-using-smart-materials-and-actuators`.

[42] Roskam, Jan: *Airplane Design*. Roskam Aviation and Engineering Corperation, 1985.

[43] Brewer, G.Daniel: *Hydrogen Aircraft Technology*. CRC Press, 1991.

[44] Khandelwal, Bhupendra et al.: "Hydrogen powered aircraft: The future of air transport". In: *Progress in Aerospace Science* (2013), pp. 45–59.

[45] Oehlke, Martin: *Massenabschätzung eines Wasserstoff-Außentanks für ein Turboprop-Ver- kehrsflugzeug*. 20099, Hamburg, 2009.

[46] Winnefeld, Christopher et al.: *Modelling and Designing Cryogenic Hydrogen Tanks for Future Aircraft Applications*. 2018.

[47] Hooker, Philip et al.: *Symposium Series No.158*.

[48] Geiß, Ingmar: *Aircraft Design Course – Introduction*. Stuttgart, Universität, Fakultät für Luft- und Raumfahrttechnik, Institut für Flugzeugbau, Vorlesungsunterlagen, 2016.

[49] Brown, Gerald ; Kim, Hyun Dae ; Felder, James: "Materials Aspects of Turboelectric Aircraft Propulsion". In: *2009 Annual Meeting Fundamental Aeronautics Program Subsonic Fixed Wing Project* (2009).

[50] Luft- und Raumfahrttechnik, Deutsches Zentrum für: *03 Raketentriebwerke-Duese-Version 2016*. 2016.

[51] San Marchi, C.: "Technical Reference on Hydrogen Compatibility of Materials". In: (2009).

[52] Institut für Antriebstechnik, DLR: "Ableitung einer Technologie-Roadmap für revolutionäre Arbeitsprozesse". In: *REVAP Abschlussveranstaltung* (2014).

[53] Tixador, P et al.: "Electrical tests on a fully superconducting synchronous machine". In: *IEEE Transactions on Magnetics* 27.2 (1991).

[54] Funke, Harald et al.: "Development and testing of a low NOx micromix combustion chamber for industrial gas turbines". In: 9 (Feb. 2017), pp. 27–36.

[55] EASA: *Certification Specifications and Acceptable Means of Compliance for Large Aeroplanes CS-25 Amendment 20.* 2017.

[56] Koroneos, Chistopher ; Moussiopoulos, Nicolas: "CRYOPLANE - HYDROGEN VS. KEROSENE AS AIRCRAFT FUEL". In: 7th International Conference on Environmental Science and Technology Ermoupolis, Syros island, Greece - Sept. 2001 (2001).

[57] Airbus: *CRYOPLANE - Final Technical Report.* 2003.

[58] Voigt, Christiane et al.: "Aircraft Emissions at Cruise and Plume Process". In: *Atmospheric Physics.* Berlin, Heidelberg, 2012.

[59] Sausen, Robert et al.: "Climate Impact of Transport". In: *Atmospheric Physics.* Berlin, Heidelberg, 2012.

[60] Faaß, Reinhard: *CRYOPLANE - Flugzeuge mit Wasserstoffantrieb.* 2001.

[61] Matthes, Sigrun et al.: "Climate Optimized Air Transport". In: *Atmospheric Physics.* Berlin, Heidelberg, 2012.

[62] Schumann, Ulrich et al.: "Contrails: Visible Aviation Induced Climate Impact". In: *Atmospheric Physics.* Berlin, Heidelberg, 2012.

[63] NASA: *N+3 Aircraft Concept Designs and Trade Studies, Final Report.* 2010. URL: https://ntrs.nasa.gov/archive/nasa/casi.ntrs.nasa.gov/20100042401.pdf.

[64] Scholz ; Gomez: "Improvements to ground handling operations and their benefits to direct operating costs". In: *2009 Deutscher Luft- und Raumfahrtkongress* (2009).

[65] Schrader, Markus: *Optimierungspotenzial des A320 Turnarounds.* 2017.

[66] Kierzkowsik, Artur ; Kisiel, Tomasz: "Conception of logistic support model for the functioning of a ground handling agent at the airport". In: *2014 Probabilistic Safety Assessment and Management PSAM* (2014).

[67] Dipl.-Ing. Kindervater, Christof: *Technologie- und Dimensionierungsgrundlage für Bauteile aus Faserverbundkunststoff (FVK).* Stuttgart, Universität, Fakultät für Luft- und Raumfahrttechnik, Institut für Flugzeugbau, Vorlesungsunterlagen, 2017.

Appendix A Gondola fuselage concept

The complementary figures are content of the lecture "Technologie- und Dimensionierungsgrundlagen für Bauteile aus Faserkunststoffverbund (FVK)" from Dipl.-Ing. Christof Kindervater, which is part of the courses at the Institute of Aircraft Design at the University of Stuttgart [67]. The lecture contains information about the gondola concept developed by the DLR under leadership of Mr. Kindervater. The final report of the research project has been published in June 2002 [23].
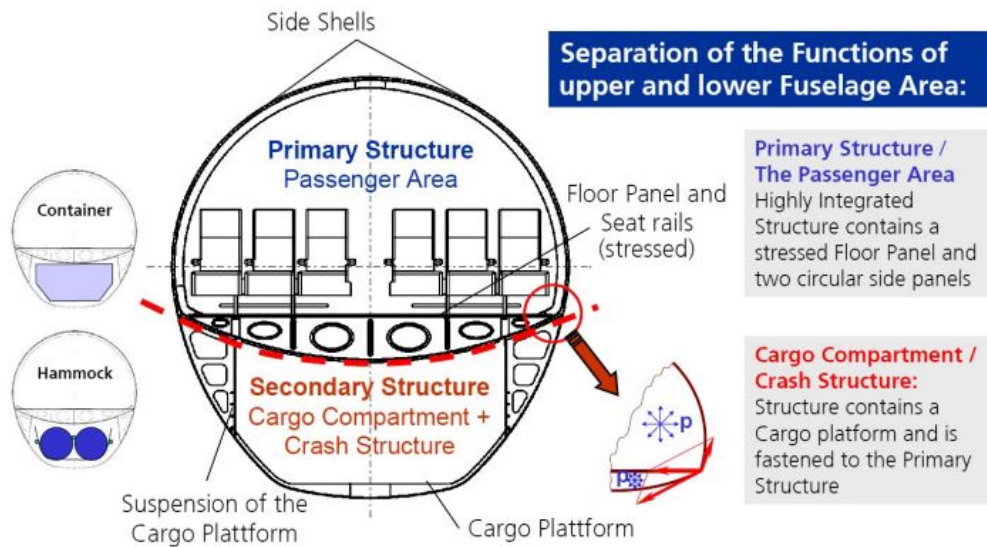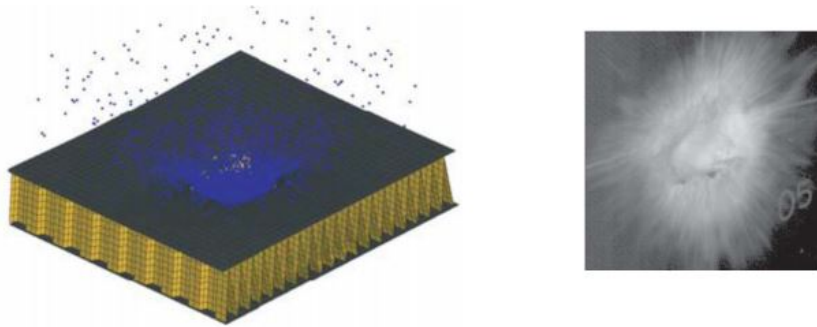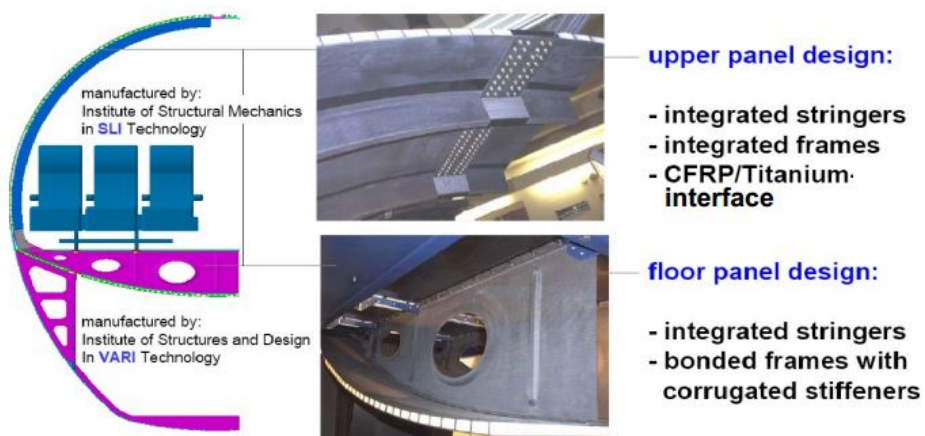
Ice impacts on VeSCo shells – simulation and test

Aspects of the fold core sandwich (VeSCo shells) under impact:
- The fold core allows buckling and therefore the outer face sheet can bend and absorb energy
- The impact energy has to be distributed over a large area, i.e. a large number of fold lines
- Fold cores show low crushing stresses
- The share of the energy absorption of the inner skin is low

Deutsches Zentrum
DLR für Luft- und Raumfahrt e.V.
in der Helmholtz-Gemeinschaft

Kindervater_FKV_CS_Schwarzer_Rumpf
Folie 27

Manufacturing

manufactured by:
Institute of Structural Mechanics
in **SLI** Technology

manufactured by:
Institute of Structures and Design
In **VARI** Technology

upper panel design:
- integrated stringers
- integrated frames
- CFRP/Titanium interface

floor panel design:
- integrated stringers
- bonded frames with corrugated stiffeners

Source: Kleineberg/DLR BS

Deutsches Zentrum
DLR für Luft- und Raumfahrt e.V.
in der Helmholtz-Gemeinschaft

Kindervater_FKV_CS_Schwarzer_Rumpf
Folie 28

Full-scale demonstrator at ILA 2002/Berlin